Developing A Localized Surface Plasmon Aptasensor for the Early Detection of Acute Myocardial Infarction

By
Makatendeka Biton

A Thesis Submitted to
Saint Mary's University, Halifax, Nova Scotia
in Partial Fulfillment of the Requirements for
the Degree of Honours in Biology.

April, 2023, Halifax, Nova Scotia

Copyright Makatendeka Biton, 2023

Approved: Dr. Christa Brosseau.
Thesis Supervisor

Approved: Dr. Ron Russell
Thesis Reader

Date: April 2023

Developing A Localized Surface Plasmon Aptasensor for the Early Detection of Acute Myocardial Infarction

By Makatendeka Biton

Abstract

Acute myocardial infarction (AMI) is a deadly disease wherein the coronary arteries become blocked, causing irreversible death to myocardial wall tissue which can result in heart failure. Current clinical methods lack the sensitivity and time efficiency needed to effectively diagnose AMI. Aptamer-based sensors (aptasensors) have been investigated as a potential rapid diagnostic technique for AMI. The high binding coefficient and selectivity of aptamers make them a desirable alternative to protein-based antibodies for developing new diagnostic platforms. Cardiac troponin I (cTnI) is one of the protein biomarkers released into the bloodstream when an AMI event occurs. Some aptasensors have been developed for cTnI detection, but not much work has used localised surface plasmon resonance (LSPR) as a sensing platform. LSPR sensing is fast, easy to use and highly sensitive to the dielectric environment on the surface of noble metal nanostructures and has shown promise for bioanalytical sensing. The objective of this thesis was to build a plasmonically active aptasensor specific to cTnI using LSPR as a proof-of-concept detection method. A glass cover slip was used as the substrate upon which silver nanostructures were assembled in a single layer using nanosphere lithography. The aptamer was immobilised onto this surface and thiols were used to fill in surface gaps to reduce non-specific binding and avoid false positives. The aptasensor was then tested to determine its ability to detect the presence of cTnI. Control measurements determined that the thiols and the aptamer did not hinder the LSPR readings. Unfortunately, the sensor could not be successfully functionalized by the aptamer because the reducing agent used in the aptamer causes delamination of the silver on the substrate and destroys

the plasmonic functionality of the sensor. More studies are needed to optimize this new sensor platform.

April 20, 2023

Acknowledgements

Firstly, I would like to thank my supervisor Dr Christa Brosseau for guiding me throughout the course of this honours project. Not only did she impart her scientific knowledge to me, but she also created an inviting environment where I felt included and supported. I appreciate all the research opportunities she offered me, and it was a great honour to be a part of her research lab. I would also like to extend my gratitude to past and present Brosseau group members who made the lab one of my favourite places to be. Many thanks to Mary Stackaruk who taught me everything I know about the PVD, Sumayyah Chotoye, Sam Julien for doing preliminary work on this research, Maddison Eisnor, Mal Hedrick, Rachel Ball, Amir Joorhab Doozha, Megan Himmelman, and Tanner George. Additionally, I would like to thank my friends for their encouragement especially Zinzile Ncube who watched all my presentations even though she did not understand.

I would also like to thank Xiang Yang for helping with all the SEMimaging that was very crucial to my thesis work. Additionally, I'd like to thank the SMU chemistry department technicians Dr. Bitu Hurisso, Dr. Najwan Albarghouthi, Dr. Elizabeth McLeod, and Patricia Granados for their support.

Above all, I would like to give my utmost gratitude to my parents for their unwavering support in all my academic and non-academic endeavours. Their love and wisdom have fueled me throughout my entire degree. I would also like to my aunt and uncle, the Kupakuwana's, who have been the ultimate parent figures for me here in Halifax. Their abundant knowledge has shaped me to be the woman I am today. I would also like to thank God Almighty who gave me the strength to overcome each obstacle that came my way.

Table of Contents

List of Figures

List of Tables

List of Abbreviations

AMI	Acute Myocardial Infarction
cTnI	Cardiac troponin I
DNA	Deoxyribonucleic acid
RNA	Ribonucleic acid
ECG	Electrocardiogram
ELISA	Enzyme Linked Immunosorbent assay
RIA	Radioimmunoassay
SELEX	Systematic evolution of ligands by exponential enrichment
PCR	Polymerize chain reaction
LSPR	Localised Surface Plasmon Resonance
NSL	Nanosphere lithography
SEM	Scanning Electron Microscope
HCP	Hexagonal close packed
SAM	Self-assembled monolayer
12-MDA	12-mercaptododecanoic acid
PVD	Physical vapor deposition
AgFON	Silver Film Over Nanosphere
AuNP	Gold nanoparticle
UV-VIS NIR	Ultraviolet-Visible-Near Infrared
BSE	Back Scattered Electron

CHAPTER 1: Introduction

1.1 Acute Myocardial Infarction

Acute myocardial infarction (AMI) occurs when the coronary arteries that supplies blood to the heart is obstructed (infarction), causing a lack of oxygen and nutrients to this tissue[1]. This can lead to tissue death of the heart muscle wall (myocardial tissue) [1]. Myocardial cell death results in the loss of cardiomyocytes which are responsible for the contractile function of the heart. Heart failure can occur as the necrotic tissue is replaced by scar tissue causing thinning of the muscle layer of the heart wall [1]. As a result, the left ventricle cavity that pumps blood away from the heart becomes enlarged making it harder for the heart to pump blood to the body [1,2]. AMI results in heart dysfunction, and eventually, if untreated, leads to death[1]. In fact, AMI is one of the leading causes of death globally, mainly affecting older individuals and younger women[3,4,5]. In Canada, AMI ranks as the second leading cause of death with about 578,000 having a history of the disease between the years 2012-2013 [5]. AMI mortality has decreased by 34.4% between the years of 2005 – 2015 and these numbers are expected to continue dropping due to improved health care service[4,5]. However, AMI remains a serious disease with a 30-day-in-hospital mortality rate around 6.3%[6] so delays in diagnosis can be fatal as the disease can further deteriorate and leave patients susceptible to other diseases [5,6].

Histological cell death of the tissue experiencing prolonged ischemia (decreased blood flow hence decreased oxygen supply) can occur very quickly[2]. For instance, necrosis of myocardial tissue can occur within twenty minutes of an artery occlusion (blocking of an artery)[2]. A study was carried out to determine the short-term survival of AMI patients in Sweden and in the UK by Chung et al [7]. The authors found that of the 119,786 AMI patients studied in Sweden, 7.6% (with

a 95% confidence interval of 7.4–7.7%) succumbed to the disease within 30 days of their AMI event[7]. In the UK, the 30-day mortality of the 391,077 AMI patients studied was 10.5% (95% confidence interval of 10.4–10.6%)[7]. Necrosis typically starts on the endocardial wall (inner layer of heart muscle/myocardial wall) and with time spreads to the epicardial wall (outer layer of the heart muscle/myocardial wall)[1]. Consequently, it is necessary to quickly diagnose and treat AMI so that necrosis is restricted to the endocardial site, which limits the deterioration of cardiac function[1]. There is strong evidence suggesting that a shorter period between diagnosis and treatment leads to a better clinical outcome of AMI treatment[1]. This indicates that there is heavy reliance on the speed and sensitivity of diagnostic methods in place that can detect AMI.

AMI symptoms typically manifest as a combination of discomfort in the upper extremities, chest, mandible, and epigastrium, shortness of breath and even fatigue [2]. Unfortunately, individuals suffering from diseases unrelated to AMI such as neurological, pulmonary, gastrointestinal, and musculoskeletal disorders can also manifest similar symptoms[2]. AMI patients may also have atypical symptoms, such as palpitations[2]. Furthermore, some AMI patients are asymptomatic, which is commonly observed in females[2]. With the wide variety of symptoms and the prevalence of asymptomatic patients, the diagnosis of AMI based on symptoms only could be challenging[2]. Subsequently, misdiagnosis or delays in treatment can occur and this can lead to grave consequences. However, AMI can also be diagnosed by looking at the physical structure of the heart and by detecting the biomarkers that are released into the bloodstream when an AMI event occurs[8,10,11].

1.2 Cardiac Troponin I

Cardiac troponin I (cTnI) is a protein with a molecular weight of 23,500 Daltons[10]. It is part of the 3-component troponin complex found in the thin filament of cardiac muscle that is responsible for the regulation of the contractile function of the heart[9]. It functions to block the myosin binding site on actin in the absence of Ca^{2+} to allow for controlled heart contractions[10]. Cardiac troponin T (cTnT) and cTnI have a specific cardiac isoform that is only found in the heart muscle whereas cardiac troponin C (cTnC) shares isoforms with skeletal muscle[9]. As mentioned before, prolonged ischemia of the myocardium results in death of the cardiomyocytes and their intracellular proteins get introduced into the blood stream[9]. cTnI is released into the bloodstream within 2-12 hours of an AMI event and can persist in the bloodstream for up to 10 days whereas troponin T is more labile[12]. It is for this reason that elevated levels of cTnI in a patient's blood is a strong indication of myocardial infarction, therefore cTnI is considered the biomarker of choice for AMI diagnosis and is regarded as the golden standard[9,10,11,12]. Normal cTnI blood concentration is 0.4 ng mL^{-1} and levels above 2 .0 ng mL^{-1} are indicative of potential disrupted function of the heart and can be directly related to myocardial injury[12]. Measuring levels of cTnI in the blood is therefore a useful tool for early diagnosis of AMI.

1.3 Diagnostic Methods for Acute Myocardial Infarction

1.3.1 Current Clinical Methods of AMI Diagnosis

Myocardial infarction is currently detected by several clinical techniques such as electrocardiography (ECG), pathology of the heart tissue, assays for detecting elevated levels of biochemical markers in the blood, and various imaging techniques[2]. An ECG is routinely required as the baseline method of detection during diagnosis of a suspected AMI event.

Electrocardiography reads the electric signals of the heart and can quickly reveal abnormalities[1]. Even so, abnormal readings can result from other heart conditions such as left ventricular hypertrophy (LVH), acute pericarditis, and stress cardiomyopathy[2]. To that end, ECGs are not sensitive, specific, or rapid enough to be the sole diagnostic tool for AMI[1,2].

Imaging techniques, such as magnetic resonance imaging (MRI), radionuclide ventriculography, and myocardial perfusion scintigraphy (MPS) are commonly used in the diagnosis of AMI[2]. Clinically, they are favored due to their ability to detect heart wall motion abnormalities, or the presence of non-viable, necrotic myocardium tissue[2]. Less commonly used techniques for AMI diagnosis include X-ray computed tomography (CT) and positron emission tomography (PET)[2]. These imaging techniques are limited because any abnormalities detected are not credited to acute myocardial infarction unless biomarker readings in the blood are above the normal range[2, 9]. Not only are these imaging techniques not specific for AMI, but they are also expensive. For communities with limited economic resources these diagnostic tools may not be available[2]. Several methods to detect cardiac biomarkers released into the blood stream following

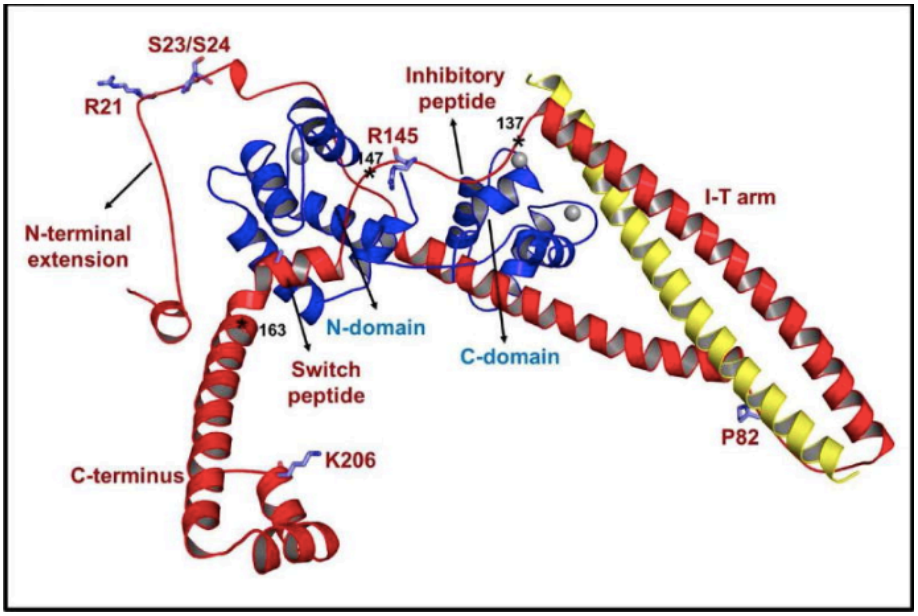

Figure 1.Ribbon diagram of cardiac troponin complex. The analyte selected for in this paper is cardiac troponin I protein shown as the red ribbon. (Reproduced with permission [9])

an AMI event have since been developed and are currently being used usually in antibody assays [10,11,12]. Detecting biomarkers is a more specific method of diagnosis that could be used in developing cheaper, more portable, and faster techniques.

1.3.2 Detecting cardiac troponin levels in the blood

To meet the need for more specific and sensitive diagnostic techniques for AMI detection, several methods have been studied and implemented for detection of cardiac biomarkers in the blood[12]. Biomarkers typically associated with AMI events include myoglobin, thrombin, cardiac troponins, and creatine kinase[11]. As mentioned above, cardiac troponin I is the gold standard for AMI detection.

Currently, blood cTnI levels are detected and monitored by enzyme-linked immunosorbent assay (ELISA) and radioimmunoassay (RIA) in clinical settings[11]. These methods are based on the selectivity of the interaction between an antigen (cTnI) and an antibody. Although ELISA has good sensitivity (limit of detection range from 6–40 pg/mL)[16], it also has disadvantages. ELISA requires pre-dilution of the samples which complicates sample preparation, has long assay running times, and has poor reproducibility[13]. Running ELISA and the process of isolating antibodies is costly, complicated and time consuming[11,12]. RIA also has its shortcomings. Though reliable, its use of radioisotopes with a short half-life introduces the need for specialized laboratories and proper waste disposal which can be costly and may not be environmentally friendly[13]. As a result, several alternatives have been developed to overcome the limitations experienced with ELISA and RIA. Techniques such as fluorescence spectroscopy, colorimetric methods, cationic isotachophoresis, and electrochemiluminescence were developed to achieve enhanced detection of cTnI in blood[9,12]. These methods are met with challenges as most of them are heavily reliant on

labelling technology, which complicates sensor fabrication and increases the sensor's reading times[12]. Aptamers have been investigated as alternatives to antibodies in diagnostic tools as they present several advantages[15]. Owing to their biomolecular makeup, oligonucleotide-based aptamers are more robust than antibodies (which are made of protein and are susceptible to denaturation) making them more attractive for use in wider varieties of assays and biosensors[15].

1.4 Aptamers for AMI biomarker detection

1.4.1 Aptamer Background

Aptamers are short single stranded DNA or RNA nucleic acid sequences that bind to a target analyte with high affinity and specificity[13,14]. Aptamers vary in length from 10-100 bases and have different three-dimensional conformations, which can be engineered and selected for to bind to a target analyte[7]. Some examples of common structural motifs of aptamers include hairpin structures, internal loops, purine-rich bulges, kissing complexes, G-quadruplex structures and stems[9]. Their lack of immunogenicity (ability of a foreign substance to invoke an immune response), their ability to undergo conformational changes, and three-dimensional folding allows aptamers to bind to a wide variety of targets[9]. Some target species that aptamers can bind to include: peptides, proteins, supramolecular complexes, small organic compounds (organic dyes, antibiotics), large molecules like glycoproteins, ions (K^+, Zn^{2+}), and even whole cells[11,12,13]. Aptamers are highly specific for their target analyte as seen in a theophylline aptamer which has a 10,000-fold discrimination against caffeine, whose only difference in chemical structure with theophylline is a methyl group[15]. Aptamers can even differentiate between isomers of the same molecule as seen with the enantiomers l-arginine and d-arginine, where the l-arginine RNA aptamer has a 12,000-fold discrimination against d-arginine[15]. Aptamers have low dissociation

constants once bound to their target analyte which means they have a high affinity for the target species owing to their folding capabilities. Aptamers can bind to their target analyte by folding to incorporate smaller analyte species into their tertiary nucleic acid structure, or aptamers can integrate into the structure of larger target species to form stable complexes[15].

Aptamers have a long shelf life and are resistant to denaturation over wider pH and temperature ranges[11,15]. Moreover, owing to their simple structure and nucleic acid composition with intra- and inter-molecular hybridization, aptamers can be used in different sensing formats[13,15]. In addition, aptamers can be regenerated more easily than antibody-based sensing platforms[13]. As a result, aptamers have found application in aptamer-based bioassays and have been used in targeted drug delivery, food analysis, imaging and tracking systems in clinical practice, molecular diagnostics, and biosensor systems especially targeted for biomarker detection[13,15].

Since aptamers are chemically synthesized, it is easy to alter their selection process to obtain aptamers that have a specific binding property or different binding properties dependent on various environments[15,17]. For example, an aptamer that can bind to a specific region of a target species can be selected for[17]. Furthermore, aptamers are not limited by immunogenicity so can be introduced into the body without inciting an immune response that could result in their degradation[17]. This allows for aptamers to have a wider range of use as opposed to antibodies which could potentially trigger an immune response and get destroyed. For example, this can allow aptamers to be applied in targeted drug delivery where it is necessary for the bound species to arrive intact at the target site. Aptamers can be synthesized in vitro whereas antibodies are produced in vitro, and this limits the range of target species for antibodies as some species may fail to initiate an immune response for antibody production[17]. Aptamers are generated by a process

called systematic evolution of ligands by exponential enrichment (SELEX) which greatly contributes to their highly specific nature[17].

1.4.2 How aptamers are isolated: The SELEX process

Systematic evolution of ligands by exponential enrichment (SELEX), first reported in 1990, is an in-vitro process used to select unique RNA/ssDNA molecules from a large combinatorial pool of random short sequences of nucleic acids[17]. The process aims to isolate a nucleic acid sequence that binds to a given target. SELEX begins with a starting pool of about 10^{14}-10^{18} unique single-stranded oligonucleotides which are preferably RNA because RNA easily folds into complex structures which are more stable than single-stranded DNA[17]. The large starting library ensures a higher probability of generating an aptamer that is specific for the target analyte of interest[15,17].

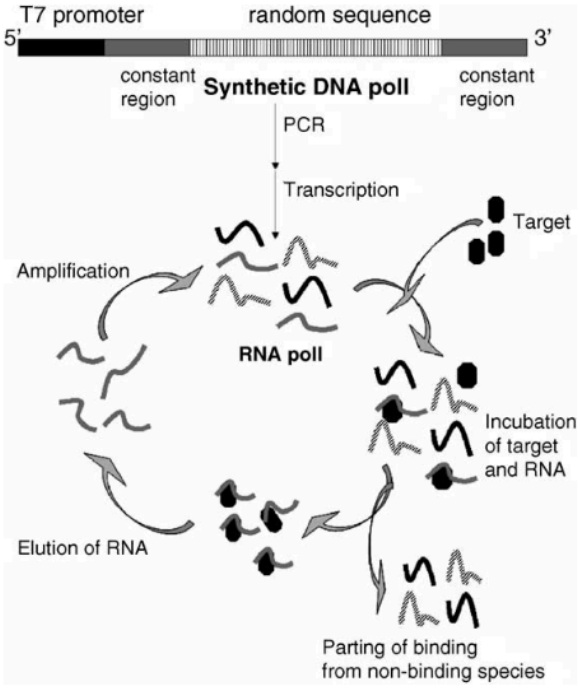

Figure 2. Schematic representation of the SELEX cyclic process for the isolation of a suitable aptamer for a specific target species. (Reproduced with permission [17])

A single-stranded DNA library is amplified by polymerase chain reaction (PCR) to give a double-stranded DNA pool which is either transcribed to give RNA or strand-separated to give ss-DNA[13,17]. Once the oligonucleotides have been converted to this form which is suitable for selection, the amplified nucleic acid library is incubated with the analyte of interest[17]. The bound aptamers are then filtered out of the reaction mixture by a nitrocellulose filter or via affinity chromatography[17]. For target molecules that are proteinacious in nature, a nitrocellulose filter is used, whereas affinity chromatography is preferred for smaller target molecules[15,17]. Unbound oligonucleotides are discarded because they have low affinity for the target analyte. The bound target is eluted to separate it from the oligonucleotides which are then amplified by RT-PCR (for RNA libraries) or PCR (for DNA libraries) to give a smaller enriched pool of potential target binding species[17]. The refined nucleic acid library undergoes the same cycle of incubation with the target analyte through to amplification (as depicted in Fig 2) about 8-15 times[17]. A negative selection step where the enriched pool is passed through the filters without analyte incubation is done to eliminate aptamers that might be binding to the adsorbent in the filter but not the target species[17]. The SELEX process has been automated and rapidly screens aptamer libraries to select a purified, high affinity aptamer at a relatively low cost[17]. This presents a major advantage over antibodies which have a complicated isolation process that can take months to complete and is expensive[15]. As a result, aptamers have been viewed as an attractive replacement to antibodies, particularly in bioanalysis as they are a suitable alternative for nearly all antibody-based designs[17].

1.4.3 Application of Aptamers- Aptasensors

A biosensor is an analytical device that can generate quantitative data about a biochemical interaction using a transducer that records changes of certain properties of a biological recognition component caused by these biochemical interactions[14]. Recently, aptamers have been used as the biological recognition element in biosensing platforms for the diagnosis of various diseases[11,13,14,15]. For example, aptamers have been incorporated in a biosensor for the detection of a tumor biomarker for cervical cancer[13] as well as in the detection of head and neck squamous cell

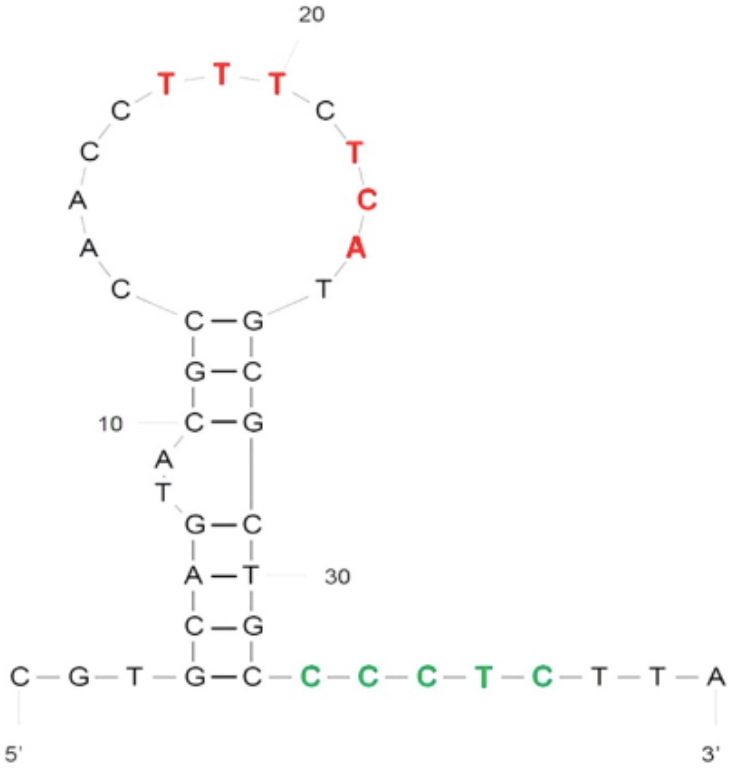

Figure 3. Diagram of the secondary structure of the Tro4 aptamer isolated by Jo et. al. DNA sequence of aptamer is as shown from the 5' to the 3' end. (Reproduced with permission [11])

carcinoma[14.] Since the isolation of aptamers for cTnI detection (particularly the Tro4 aptamer)[11], aptasensors for acute myocardial infarction have been developed using various sensing platforms. Several biosensing methods for cTnI detection have been investigated including strip voltammetry,

cyclic voltammetry, electrochemiluminescence, colorimetry, and fluorescence-based biosensors[14]. These studies were successful in detecting cTnI and are being vetted for clinical application. Other sensing platforms use optical properties such as localized surface plasmonic resonance (LSPR) which has advantages of simplicity, cost efficiency, fast response and sensitivity[13, 14,18,19]. LSPR sensing has been successfully applied in the detection of several diseases including cancers [13,14], but there have been no reports of application in the detection of cTnI for AMI diagnosis. This thesis research aims to explore LSPR as a sensing platform for detection of cTnI using Tro4 aptamers as the biological recognition element.

1.5 Preliminary work on aptasensor detection of cTnI

A previous honours student in the Brosseau group, Sam Julien, carried out research work that formed the foundation of this thesis work[20]. Their research sought to develop an aptasensor using electrochemical surface-enhanced Raman spectroscopy (EC-SERS) as a probe for AMI diagnosis. EC-SERS is an analytical technique used to measure the Raman spectra (molecular vibrational fingerprint) of a molecule adsorbed to an electrode[20,21]. EC-SERS can measure the presence and concentration of an analyte in solution by monitoring changes in the Raman spectra when a voltage or current are applied[21]. Julien prepared a ternary (three part) monolayer on a carbon screen printed electrode (coated with silver nanoparticles) comprised of the Tro4 aptamer and thiol backfilling agents as the aptasensor. The backfilling agents are used to prevent non-specific binding of non-target or unbound analyte which could produce inaccurate results. Nucleotide base control studies performed in their thesis work proved that the aptamer was appropriately immobilised onto the surface of the sensor via a 6-carbon thiol linker and not lying flat on the surface which would be unfavourable[20]. Studies to assess effectiveness of the blocking

agents to prevent adsorption of non-target species gave a >99% signal blocking efficiency[20]. Additionally, studies were performed to show that the aptamer remained immobilised on the surface of the sensor after modification with the thiol back filling agents[20]. The optimized procedure for building the ternary monolayer reported by Julien was used to build the LSPR aptasensor in this thesis work[20].

Although Julien successfully optimized the functionalization of the cTnI aptasensor, they were unable to detect the cardiac troponin I analyte using EC-SERS [20]. It was reported that there was apossibility that upon introduction of the electrolyte, the cTnI was desorbing from the electrode surface and going into solution[20]. Additionally, the distance between the protein binding site on the aptamer and the plasmonic electrode surface is approximately 11.7 nm[20] which is beyond the field of sensitivity for this detection method. Correspondingly, a replacement sensing method with a longer penetration depth was needed to continue this work. Localised surface plasmon resonance sensing uses changes in refractive index experienced in their dielectric environment to detect an analyte. The penetration depth for LSPR is reported to be >10 nm [23] from a plasmonic surface and so this detection method was determined to be a suitable replacement for EC-SERS to continue this work.

1.6 Localized Surface Plasmon Resonance (LSPR)

Localized surface plasmon resonance (LSPR) is a phenomenon that is generated when incident photon frequencies are in phase with oscillating electrons within noble metal nanoparticles[18,19]. When the incident light wavelength is longer than the size of a metallic nanoparticle, the free electrons in the metal particle polarize, leading to a plasmon (a quasiparticle of plasma energy) that oscillates around the nanoparticle (Fig 18)[18]. The plasmon oscillation

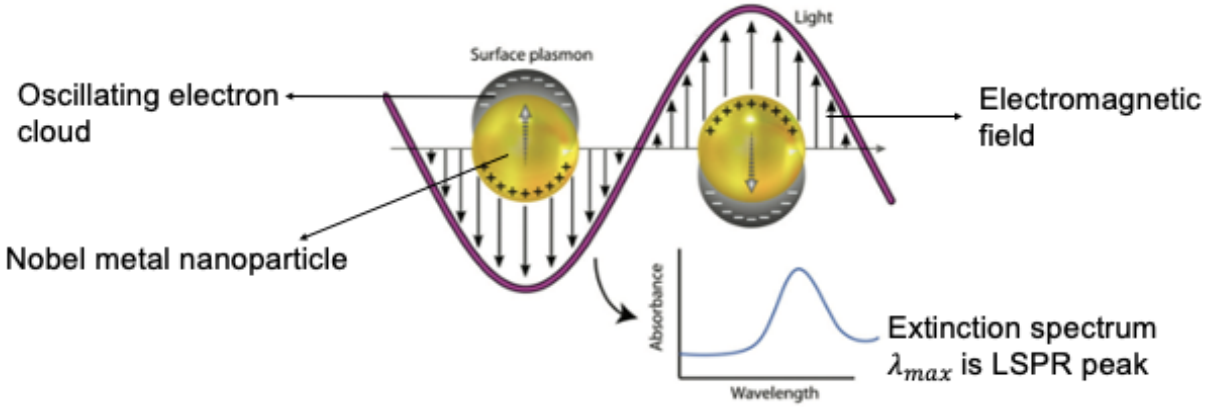

Figure 4. Schematic of oscillation of nanoparticles which create an electromagnetic field that is called the localized surface plasmon. (Reproduced with permission[22])

creates an electromagnetic field around the nanoparticles which is highly sensitive to any changes that occur in the surrounding dielectric environment[13,18]. A dielectric environment is a non-conductive medium and in LSPR it assists with confining the electromagnetic field to a region close to the surface of the nanoparticles[18,23]. This region is relatively short in LSPR and allows monitoring of short-range changes in the refractive index which are usually caused by molecular adsorption[18,23]. The excited plasmons produce an extinction spectrum (see Fig4) which shows the change in absorption and scattering of the incident light passing through or being reflected from the surface of the sample in the UV-Visible near infra-red region[18]. The λ_{max} of the extinction spectra is denoted the LSPR peak[13, 18, 24].

The plasmon resonance conditions can be shifted when a change is experienced in the dielectric environment[13,18]. These changes in the dielectric environment are indicative of a biochemical reaction such as the adsorption of a molecule onto the plasmonic surface or binding of a species to a capture agent immobilised on the surface. The interaction of adsorbed molecules with the electromagnetic field can be observed in three modes namely angle resolution, imaging, and wavelength shift[18]. In angle resolution, the reflectivity of the light is observed as a function of its angle of incidence with the plasmonic surface. In this mode, the wavelength is kept constant. In imaging, both the wavelength and angle of incidence are kept constant, and the reflectivity of a sample is measured as a function of position[18]. Using the wavelength shift mode, the angle of incidence is kept constant, and the reflectivity of the light is observed as a function of the wavelength[18]. Put simply, the reflectance is measured as the dependant variable along the electromagnetic spectrum which is the independent variable. The simplicity of the wavelength shift mode makes it the mode of choice for observing and quantifying biochemical interactions[18,24].

The wavelength of the LSPR peak prior to sample introduction usually shifts to the red region (longer wavelengths) of the electromagnetic spectrum in a sample reading[18]. The shift in the wavelength is caused by a change in the refractive index at the metal surface due to the introduction of the analyte[18,22]. This sensitivity to changes in the dielectric environment make LSPR very attractive as a sensing platform for detecting low concentrations of target analytes in food safety, environmental protection, and disease detection[19].

As previously discussed, LSPR has been used as a sensing platform for the detection of biomarkers of diseases in aptasensors and have competitive limits of detection compared to techniques such as ELISA[12,13,14,18,19]. To make an LSPR sensor, a plasmonic base is required as the detection device and surface chemistry is required for capturing of the analyte of interest[22].

Several methods exist for fabrication of metal nanoparticles of different shapes and sizes. Nanoparticle structures can be synthesized chemically or lithographically. In chemical synthesis, large amounts of the nanoparticles can be produced, but lithographic techniques present the advantage of flexibility in making precise shapes and arrangement of the nanometals[18]. Lithographic techniques include nanosphere lithography (also known as colloidal lithography) which can produce different substrate masks and electron beam lithography[18,22]. Nanosphere lithographic techniques are favoured as they are inexpensive, faster, and easier to use than electron beam lithography. In nanosphere lithography (NSL), a colloidal suspension of nanospheres is deposited onto a surface allowing the nanospheres to self-assemble in a monolayer (colloidal mask)[18]. This mask can be used in one of three ways to achieve the desired plasmonic nanometal structures. In one method, a thin film of a noble metal (15 nm -100 nm thick) can be deposited onto the mask then dissolve the spheres to give an array of triangular metal nanoparticles (hexagonal close packed (HCP) nanostructures)[18,25].

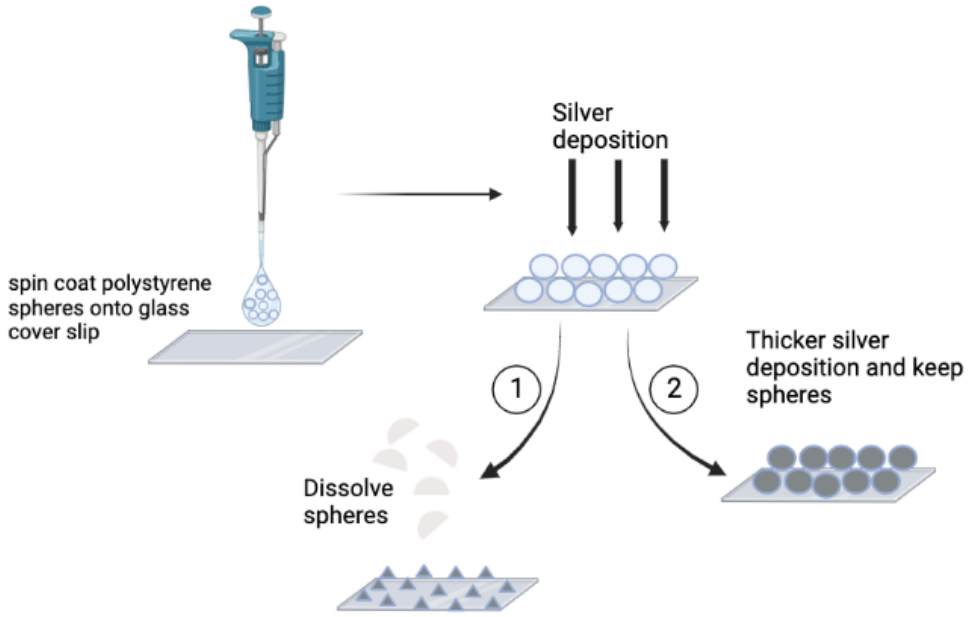

Figure 5. Schematic showing components of aptasensor with cardiac troponin I captured by aptamer

In a different approach, small wells (where the metal can be deposited) can be made over top of the colloidal mask can using reactive-ion etching. A third approach would be to deposit a thicker layer of metal on the colloidal mask (about 200 nm) to create metal film over nanosphere (FON) substrates[18,24,25]. A schematic of the steps of fabricating AgFON and HCP substrates is shown in Figure 5. These plasmonic surfaces with the metal nanoparticles can be modified with molecular receptors for analyte capture such as antibodies, aptamers and even enzymes[22].

LSPR sensors using aptamers as a capture agent have been successfully developed for the detection of biomarkers for various diseases as mentioned in section 1.3.3. These sensors have produced competitive limits of detection compared to previously mentioned spectroscopy techniques and have good reproducibility. For example, an LSPR sensor to detect a biomarker for Alzheimer's disease, amyloid-beta-derived diffusible ligand, was developed using a sandwich format assay with antibodies[18]. The system was able to detect analyte concentrations in the 100 fM range[18]. In another study, NSL was used to make an array of silver triangular nanoparticles that were then modified with monoclonal anti-squamous cell carcinoma antibody for cervical cancer diagnosis[13]. A dynamic linear range of 0.1–1,000 pM of the analyte was reported and the authors were even able to regenerate the sensor for reuse by incubating the used sensor in a low pH solution[13]. Following this, the concentration of cTnI in patient and non-patient blood reported in section 1.2 coincides with the dynamic linear range of LSPR reported in numerous studies and is above the limit of detection of LSPR sensing. As such, LSPR could be used to develop a robust and cheap sensor that could be used in point of care diagnosis of AMI.

1.7 Scope of thesis

This research seeks to combine the simplicity and sensitivity of LSPR with the selectivity and durability of aptamers to develop a robust sensor to detect cTnI for AMI diagnosis. Since the Tro4 aptamer is highly specific for its target molecule, there is confidence that any changes experienced in the LSPR peak shift are due interaction of the aptamer with the target analyte. The objectives of the thesis research are as follows:

- Fabricate a plasmonically active sensor base that produces an extinction spectrum with the characteristic LSPR peak
- Functionalize sensor base with aptamer and thiol backfilling agents
- Perform control experiments to determine how each component of the sensor affects the LSPR peak
- Perform experiments with standard cardiac troponin I protein

It is hypothesized that an LSPR-based sensor can be used for acute myocardial infarction diagnosis by detecting circulating cardiac troponin I using a Tro4 aptamer as a capture agent.

CHAPTER 2: EXPERIMENTAL MATERIALS AND METHODS

2.1 Standard protocol

All chemicals were used without further purification unless otherwise stated. The water used for rinsing glassware and aqueous solution preparation was Millipore water (resistivity >18.2 MΩ cm). All glassware used during experiments was soaked in neat sulfuric acid for a minimum of 4 hours and rinsed 30 times with Millipore water prior to use.

2.2 Fabrication of localised surface plasmon resonance (LSPR) based biosensor

The biosensor was fabricated to have a plasmonically active base made by depositing metal nanostructures developed using nanosphere lithography. Three types of metal nanostructures for the plasmonic sensor base were investigated: hexagonal close packed silver nanotriangles, gold nanoparticles, and silver film over nanospheres (AgFONs). These were compared to determine the nanostructure that would produce the best LSPR signal with the instrument set up used in this research. A ternary monolayer consisting of the aptamer and thiol blocking agents was built onto this plasmonically active base using an optimized method[20]. First the Tro4 aptamer (capturing agent) was immobilized onto the plasmonic base then thiol back-fillers were used to fill in spaces between the aptamers (Fig6). A schematic of each of the components of the sensor is shown in Figure 6. In this section, the steps of the sensor assembly are discussed in detail.

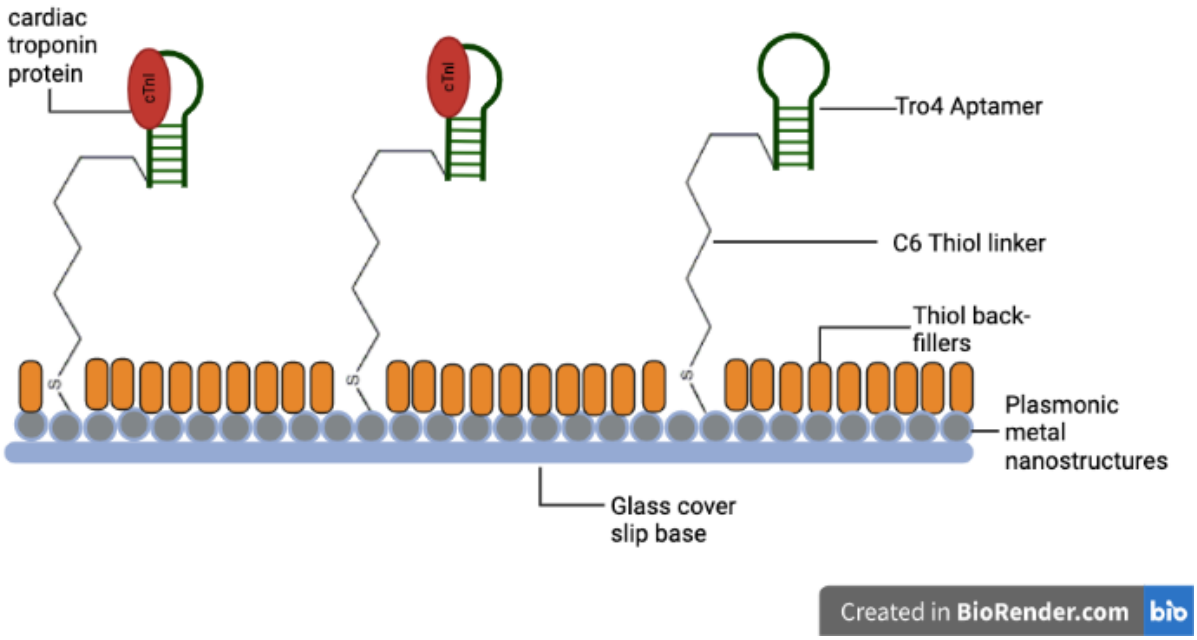

Figure 6. Schematic showing components of aptasensor with cardiac troponin I captured by aptamer (size of structures not shown to scalar ratios)

2.2.1 Cleaning the coverslips

The nature of this sensor is based on surface chemistry and as such is highly sensitive to contamination. The coverslips were cleaned prior to building the sensor to ensure that they were free of impurities and contaminants which could potentially interfere with readings. 18 mm and 12 mm circular micro cover glasses purchased from VWR (Radnor, PA, USA) were soaked in 20 mL of piranha solution (3:1 H_2SO_4 : H_2O_2) for thirty minutes then rinsed with Millipore water. CAUTION: Piranha solution is an extremely corrosive substance in liquid and vapor form. As such, the chemical must be handled in the fume hood, direct contact with skin must be avoided, and correct personal protective equipment must be worn. The sulfuric acid (96%) used was purchased from ACP Chemicals (Montreal, Quebec, Canada) and hydrogen peroxide (30%) ACS grade was purchased from Fisher Chemicals (Ottawa, ON, Canada). It is necessary to make the glass surface hydrophilic for the polystyrene spheres to move freely across the glass cover slip

surface for an improved arrangement of the spheres. To make the cleaned surface hydrophilic, the coverslips were sonicated for an hour in an etching solution of 15 mL Millipore water, 5 mL ammonium hydroxide (28-30%) (ACS Plus grade purchased from Fisher Chemicals (Ottawa, ON, Canada)) and 5 mL hydrogen peroxide. All sonication processes were carried out in a fume hood using the 3210 Brasonic® Ultrasonicator (Laramie, WY, USA). The etched cover slips were then thoroughly rinsed with Millipore water, stored in a beaker with 100 mL of Millipore water, and covered with parafilm to prevent evaporation. All cover slips were used within 3 - 4 weeks after which they would need to be re-cleaned and re-etched prior to use.

2.2.2 Nanosphere Lithography

The nanosphere lithography method reported herein was adapted from the work of the Van Duyne group[25]. In an Eppendorf tube, a polystyrene solution was prepared according to the ratios listed in Table 1. 0.5g of 0.503 μm polystyrene spheres suspended in water were purchased from Bangs Laboratories Inc (Fishers, IN, USA). ACS grade ethylene glycol (>95%) was purchased from Fisher Chemicals (Ottawa, ON, Canada). Alkyl-aryl polyether alcohol (TX-100) (a surfactant) was purchased from JT Baker Chem Co. (Phillipsburg, NJ, USA). The surfactant was explored as it could slow down the evaporation rate of the sphere suspension while also improving its wettability. This could result in a more even deposition of the spheres across a surface. Methanol was purchased from Commercial Alcohols by Greenfield (Brampton, ON, Canada).

The sphere suspension was deposited onto the clean cover slips to give a self-assembled monolayer of polystyrene spheres by four different deposition methods to determine which maximized coverage of polystyrene spheres on the coverslip surface. The best deposition method was determined first and then using that method, the mixtures in Table 1 were investigated to determine the optimum mixture for the sphere depositions. The criterion for a good deposition

method is one that would give a monolayer of the deposited polystyrene spheres, and this was determined by scanning electron microscope (SEM) imaging.

Table 1. List of ratios of polystyrene sphere solutions used for sphere depositions.

Solution	Volume deposited
1:1, spheres:TX-100/meOH	10 μL, 15 μL, 20 μL
2:1, spheres:TX-100/meOH	10 μL, 15 μL, 20 μL
3:1, spheres:TX-100/meOH	10 μL, 15 μL, 20 μL
1:1, spheres: meOH	10μL, 15μL, 20μL
1:1, spheres: ethylene glycol	15 μL
spheres only	7 μL, 10 μL

Manual deposition - Tweezers were used to obtain a clean cover slip from the beaker then dipped in freshly obtained Millipore water in a separate beaker. To drain excess water, the edge of the coverslip was touched to a Kim-wipe™ which wicks away excess water. 4 μL of the sphere solution was deposited onto the coverslip with a micropipette. The coverslip was then held with tweezers and rotated to spread the solution onto the surface for approximately 6 minutes or until dry.

Deposition using the Orbital Shaker- A Kim-wipe™ was taped to the platform of the orbital shaker and a piece of double-sided tape was placed on top of the wipe. A clean coverslip was extracted using tweezers, dipped in fresh water then dabbed dry on one side. The coverslip was placed onto the piece of tape wet face up and 3 μL of the sphere solution was deposited on the

coverslip. The orbital shaker was immediately turned on to a speed of 6 rpm to disperse the sphere solution on the coverslip for approximately 10 minutes.

Deposition using Roto-Mini - Double-sided tape was placed on the instrument as shown in Figure 7 while positioned in a horizontal fashion. A clean coverslip was retrieved as described

Figure 7. Image of the RotoMini with a glass cover slip attached by double sided tape (circled in red)

above and placed onto the piece of tape. 3 μL of the sphere solution was deposited onto the coverslip and the instrument was immediately switched on. The Roto-Mini was allowed to rotate for 10 minutes at its one speed setting of 24 rpm.

Deposition by centrifugation- To mimic the process of spin coating, a one speed (6000 rpm) MyFuge™ minicentrifuge type C1008-R by Mandel (Guelph, ON, Canada) was used. A small square of double-sided tape was placed onto the centre of the centrifuge. A clean coverslip

was retrieved and placed on the piece of tape. Immediately, 7 - 20 µL of the sphere solution was deposited onto the cover slip at 6000 rpm for 30 seconds.

2.2.3 Physical Vapor Deposition of Silver (Ag) Film

Thin silver (Ag) films were deposited onto the nanosphere lithography masks using physical vapor deposition (PVD). The PVD instrument was the COVAP 2000, manufactured by Angstrom Engineering and the silver pellets used in the deposition were 99.999% purity, 1/8" x 1/8" purchased from Angstrom Engineering (Kitchener, ON, Canada). The controlled deposition

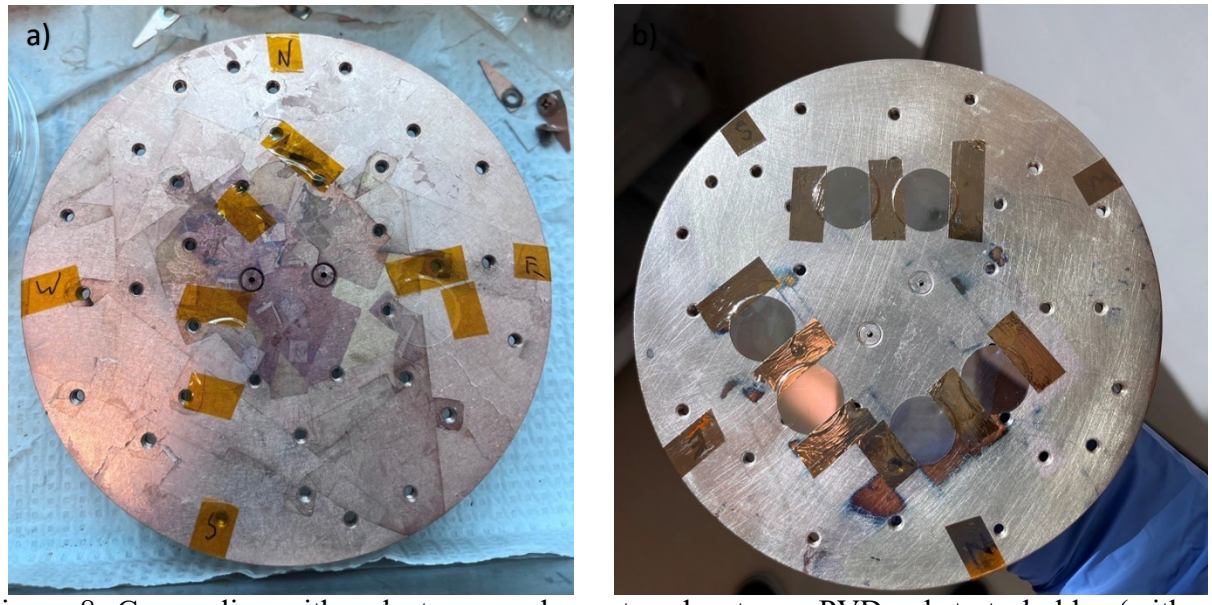

Figure 8. Cover slips with polystyrene spheres taped onto on PVD substrate holder (with Kapton tape). a) samples prior to silver deposition, b) after silver deposition

of silver was monitored by a 6 MHz gold coated quartz crystal microbalance (QCM sensors, Lytron MCS Modular Cooling System) which maintains the set thickness and a deposition rate of 2.0 Å/s. For accurate depositions, the quartz crystal was monitored as its accuracy at reporting the quality of the deposition is best above a crystal life of >80%, otherwise the crystal was replaced with a new one. For silver deposition, the system maximum power was set to 40% and the tooling factor

was set to 35%. The nanosphere lithography masks were mounted onto the substrate holder using Kapton tape purchased from Uline (Milton, ON, Canada), as shown in Figure 8. The substrate holder was marked with coordinate points to allow for identification of the substrates post Ag deposition. The thickness of the silver film varied from 20 nm to 50 nm to determine which would give a better LSPR signal.

2.2.4 Dissolving Polystyrene spheres to give Hexagonal-Close-Packed Monolayer

The polystyrene spheres on the Ag-coated masks were dissolved in three different solvents to produce hexagonally arranged triangular Ag nanoparticles which shall be referred to as HCP masks (hexagonal-close-packed masks). The various solvents explored to dissolve the spheres were toluene, ethylene glycol and 10% dichloromethane in hexanes, all purchased from Fisher Chemicals (Ottawa, ON, Canada), and ethanol (>95%) purchased from Commercial Alcohols by Greenfield (Brampton, ON, Canada). In a fume-hood, the sonicator was set-up and degassed for twenty minutes. Approximately 5-10 mL of solvent was poured into a beaker and placed in the sonicator bath with the support of a clamp stand. The Ag-coated mask was placed into the beaker and sonicated for varying times of 1 min, 1.5 min, 2 min, and 2.5 min to determine which time was best for dissolving the polystyrene spheres. The resulting HCP mask was retrieved from the beaker with tweezers, rinsed with fresh solvent (to remove trace polystyrene spheres), and was placed on a Kim-wipe ™ in a petri-dish to air dry in the fume-hood. It was found that sonication in the toluene solvent worked best to effectively dissolve the polystyrene spheres and so this method was used for the rest of the sensors made in this thesis work.

2.2.5 Functionalization of HCP masks

The HCP masks were functionalized by the aptamer first followed by a self-assembled monolayer (SAM) of two thiol backfilling agents namely 12-mercaptododecanoic acid (12-MDA) and cysteamine.

Immobilizing aptamer onto HCP mask- The oligonucleotide used was the tro-4 aptamer which was purchased from Integrated DNA Technologies Canada (Toronto, ON, CA). The sequence of the tro-4 aptamer is as follows:

5'-/5ThioMC6-D/-CGTGCAGTACGCCAACCTTTCTCATGCGCTGCCCCTCTTA-3'

The aptamer was shipped in the more stable disulfide form denoted D in the sequence above and the 5' end was modified to contain a 6-carbon thiol linker to allow the aptamer to bind to the silver substrate surface via an Ag-S bond (denoted 5ThioMC6 in the sequence above)[26]. The aptamer was shipped in its oxidised form (disulphide, S-S) to protect the sulphur atoms because the thiol group is unstable over extended periods of time[27]. To reduce the disulfide bond to give the S-H functional group, 1 μmol aptamer was allowed to thaw and 100 μL of 1.0 M tris(2-carboxyethyl)phosphine hydrochloride (TCEP) (≥98%) purchased from Sigma-Aldrich (St, Louis, MO, USA) prepared in Millipore water was added to the tube with the aptamer[3]. The solution was incubated at room temperature (22-25ºC) for 2 hours to allow the aptamer to be fully reduced, then stored in the fridge (2-8 ºC). The TCEP acts as the reducing agent that will break the S-S bond and give two thiol groups[27]. The reduced aptamer was used as is, and the TCEP solution was not removed before use[27]. To immobilize the aptamer onto the surface of the HCP mask, 10 μL of the reduced aptamer was drop-coated onto its surface. The reduced aptamer was carefully spread on

the surface of the HCP mask by using the tip of the micropipette tip, taking care not to scratch the substrate. The treated HCP mask was allowed to dry overnight in the fume hood at room temperature.

Backfilling with thiols- The aptamer immobilized onto the sensor base is bulky and so gaps are present between the aptamers. Non-specific binding of foreign/matrix substances onto these gaps can result in false positive signals[26]. To avoid this, the gaps on the sensor substrate need to be filled in by a process called backfilling where the sensor chip is allowed to incubate with thiol molecules that can bond to the silver surface via a strong Ag-S bond [26,28]. The thiols selected for backfilling were 12-mercaptododecanoic acid (12-MDA) (96%) which can fill large spaces due to its long carbon chain and cysteamine (≥98%) to fill in the smaller gaps[20,26,28]. Both reagents were purchased from Sigma-Aldrich (St, Louis, MO, USA). The method for backfilling was adapted from the previous work of Julien. The aptamer-modified HCP mask was immersed in a solution of 5.0 mM 12-MDA in methanol and incubated for 2 hours at room temperature. The mask was retrieved, rinsed with methanol, and allowed to air dry in the fume-hood for about 5 minutes. The mask was then incubated in a solution of 5.0 mM cysteamine dissolved in Millipore water for 30 minutes at room temperature. The SAM-modified mask was then rinsed with Millipore water and allowed to air dry in the fume hood to give the fully functionalized mask with the ternary monolayer.

2.3 Making a AuNP LSPR active sensor

2.3.1 Gold nanoparticle synthesis

The gold nanoparticle (AuNP) synthesis method used herein was followed as reported by Ji et.al.[29] The 250 mL three-neck flask used for this experiment was cleaned with aqua regia, rinsed with copious amounts of ultrapure water, and allowed to dry completely prior to the experiment. The aqua regia was a 3:1 v/v of trace metal grade hydrochloric acid (34-37%) and trace metal grade nitric acid (67-70%) both purchased from Fisher Chemicals (Ottawa, ON, Canada). CAUTION: Aqua regia is a potentially explosive and extremely corrosive substance in liquid and vapor form. As such, the chemical must be handled in the fume hood, direct contact with skin must be avoided, and correct personal protective equipment must be worn. 100 mL of a 0.25 mM aqueous solution of hydrogen tetrachloroaurate ($HAuCl_4$) (99.8%) purchased from STREM Chem Inc. (Newburyport, Massachusetts, USA) was added to a flat bottomed 3-neck flask wrapped in aluminium foil. The solution was brought to a boil with stirring under reflux. A solution of aqueous 5% sodium citrate purchased from Sigma-Aldrich (St, Louis, MO, USA) was made and 1 mL of the solution was added to the boiling flask. The reaction mixture was allowed to boil for 20 minutes or until the solution turned wine red (colour of AuNP). The nanoparticle mixture was allowed to cool to room temperature.

2.3.2 Assembling the AuNP sensor chip

The method used to make the AuNP sensor chips was modified from Oh et. al[30]. Piranha-cleaned glass coverslips were immersed in a 1% 3-aminopropyl-triethoxysilane (≥98%) (APTMS) methanolic solution and allowed to incubate for 2 hours. This treatment was done to allow the

AuNP to adhere to the glass surface via strong Au-S bonds. The APTMS was purchased from Sigma-Aldrich (St, Louis, MO, USA). The coverslips were then rinsed with methanol to remove excess unbound APTMS and allowed to dry. The coverslips were then incubated in a suspension of AuNP at room temperature for 16 hours in one experiment, and 24 hours in another. The 16 hour and 24-hour incubation LSPR active coverslips were then rinsed with ultrapure water and allowed to dry.

2.4 Making Silver film over nanosphere (AgFON) substrates

AgFONs were made using a modified version of the protocol reported by Lee et. al[24]. Glass coverslips used for this experiment were cleaned using the method in section 2.2.2. 0.503 μm polystyrene spheres purchased from Bangs Laboratories Inc (Fishers, IN, USA) were deposited onto the glass surface using spin coating (modified centrifugal deposition as described in section 2.2.3). 250 nm of silver was deposited onto the substrates at a deposition rate of 2.0 Å/s using the PVD. The resultant AgFONs were stored in the dark at room temperature.

2.5 Preparation of cardiac troponin I (cTnI) protein

The recombinant cardiac troponin I protein was purchased from MyBioSource (San Diego, CA, USA) at an initial concentration of 0.621 mg/mL and stored in the freezer. 0.05 mg of the protein was in an 80 μL solution of containing 6.0 M urea and 50 mM tris buffer pH 8. Potassium phosphate dibasic (≥98%) purchased from Anachemica Canada (Montréal, QC, CA) and potassium phosphate monobasic (≥99%) purchased from Sigma-Aldrich (St, Louis, MO, USA) were used to make a pH 7.4 phosphate buffer. The buffer solution was used to dilute an aliquot of the cTnI protein solution in a separate Eppendorf tube to achieve a concentration of 250 μg/mL.

For all measurements with the protein, 10 μL of the diluted protein solution was pipetted onto the modified sensor and allowed to stand for an hour. After this time had elapsed, the sensor was rinsed with Millipore water to remove excess protein not bound by the aptamer and allowed to air dry completely before proceeding with LSPR measurements.

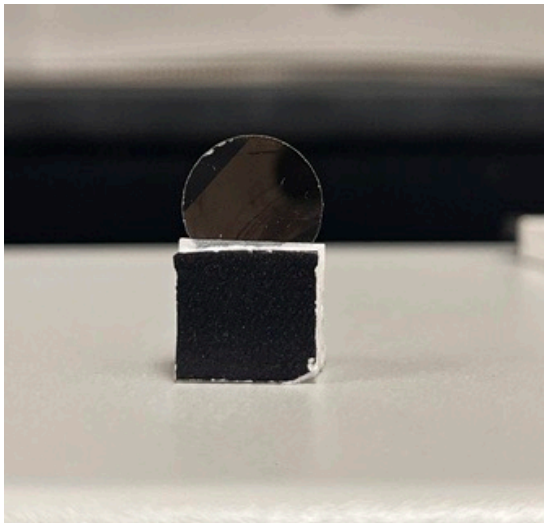

Figure 9. Sensor chip inserted in a lab-made substrate holder made of Styrofoam and painted black to avoid refraction errors.

2.5 LSPR measurements

All LSPR measurements were taken using an Ocean Optics USB2000+ UV-VIS NIR spectrometer equipped with a deuterium and a halogen lamp light source as well as a linear array CCD detector. The set-up had a 1cm cuvette holder and the software used to record the data was OceanView 2013 version 1.6.7. A self-made substrate holder was fashioned from foam to allow the substrate to stand upright while the incident light shone through it (Figure 9). Measurements were taken either in the transmission mode (for the HCP masks and AuNP substrates) or in reflectance mode (for the AgFONs). Both lamps were used with acquisition times of 1 ms, 2 ms and 5 ms at 1 scans to average. Scans to average is the number of spectral acquisitions the spectrometer will collect before averaging the data. Measurements were done in the dark to avoid

interference from external light sources. All optimized HCP masks, AgFONs and AuNP LSPR active sensor chips were measured to compare their LSPR signals. Collected data was analyzed using Origin 2020b Software (OriginLab Corporation Northampton, MA, USA).

2.6 Scanning Electron Microscope (SEM) studies

To evaluate the distribution of the polystyrene spheres on the surface of the coverslip, a TESCAN MIRA 3 LMU Variable Pressure Schottky Field Emission Scanning Electron Microscope (FE- SEM) with a maximum resolution of 1.2 nm at 30 kV was used. The sensor chips were imaged after the silver deposition and were prepared on carbon tape to reduce charging. The HCP masks could not be examined on the SEM due to charging caused by the exposed glass after dissolving the polystyrene spheres. To evaluate if the nanosphere lithography process gave hexagonally arranged triangular nanostructures, the process was performed on atomically flat silicon wafers. The use of silicon wafers was necessary because unlike the glass coverslips, they

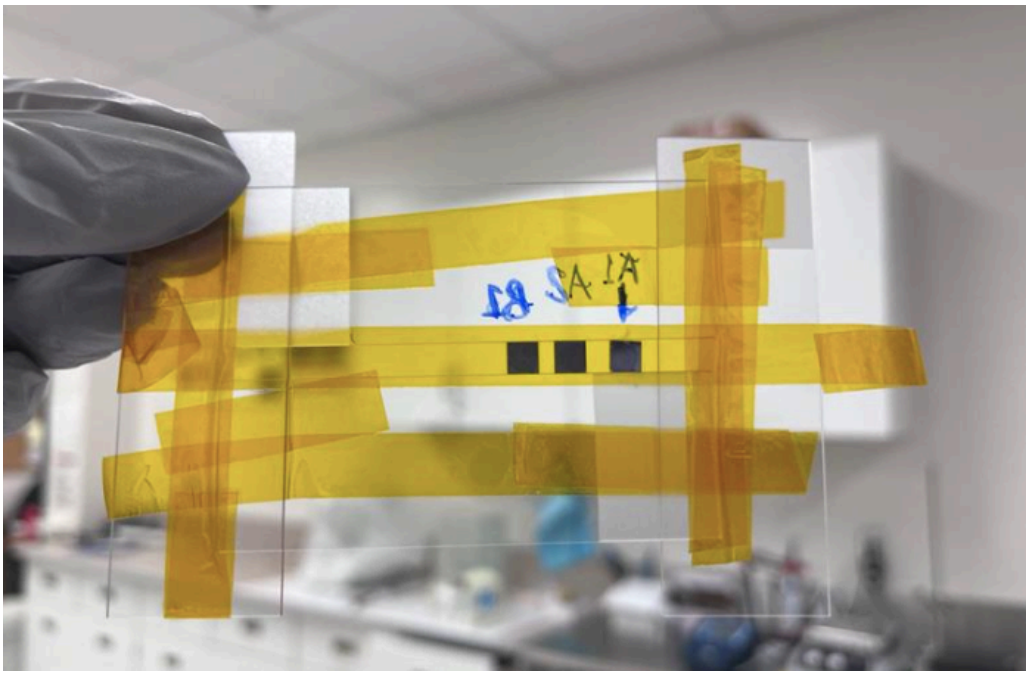

Figure 10**.** PVD substrate mask for silicon wafers made from glass coverslips held together by Kapton tape.

do not cause charging issues in the SEM instrument after dissolution of the polystyrene spheres which could result in poor SEM images.

To do this, 4-inch silicon wafers in 5 x 5 mm chips purchased from Ted Pella Inc (492477, Redding, CA) were washed by sonicating for 5 min in acetone and immediately rinsed with isopropanol to avoid residues. The wafers were allowed to air dry completely before depositing 5 µL of the sphere solution by the spin coating process (Section 2.2.3). A mask fashioned from generic glass slides purchased from VWR (Radnor, PA, USA), was assembled using Kapton tape to hold the silicon wafers during Ag deposition (Figure 10). The polystyrene spheres on the silicon wafers were dissolved in toluene as described in section 2.2.4 and the resulting wafer HCP mask was prepared on carbon tape for SEM imaging. SEM image processing to determine percent coverage of the polystyrene spheres was done using the INCA® software suite version 4.15 (England, UK).

CHAPTER 3: RESULTS AND DISCUSSION

Acute myocardial infarction is the second leading cause of death in Canada and is highly misdiagnosed due to atypical symptoms[5]. Current diagnostic methods based on physical symptoms of AMI are not unique to AMI diagnosis as these symptoms are indicators of other diseases as discussed in section 1.3.1. Cardiac troponin I (cTnI) is identified as the golden standard for AMI diagnosis as it is a biomarker highly specific to AMI events[10]. Methods to detect cardiac troponin such as ELISA and RIA are currently in use but lack the efficiency and flexibility to make AMI diagnosis faster, cheaper, and less complex[11,13]. Aptamer based sensors (aptasensors) for AMI diagnosis using localised plasmon resonance (LSPR) sensing as a probe for quantification have not been explored. LSPR provides an easy, sensitive, rapid, and reproducible means of converting the biomolecular interactions into analytical data[18]. For this thesis, it was hypothesized that a localised surface plasmon resonance-based sensor can be used for early diagnosis of acute myocardial infarction using an aptamer as a capture agent.

3.1 Polystyrene sphere deposition optimization

To test this research hypothesis, a plasmonically active sensor base was built to quantitatively detect cTnI by analysing the LSPR peaks before and after deposition of the analyte. To make a plasmonically active sensor base, metal nanostructures were fabricated on glass coverslips. Polystyrene spheres were deposited as a sacrificial mask for the hexagonal-close-packed (HCP) monolayer or as a scaffold for the film over nanosphere (AgFON) type sensor. For both, it was equally important that the polystyrene spheres be deposited in a single compact monolayer to achieve the desired shape in HCP type and to produce a uniform LSPR signal.

3.1.1 Polystyrene sphere deposition methods

Several polystyrene sphere deposition methods were tested, and the resulting substrates are shown in Fig 11. The hand/manual (Fig 11a), orbital shaker (Fig 11b), and Roto-Mini (Fig 11c) depositions show uneven distribution of the spheres. The centrifuge deposition substrate provided

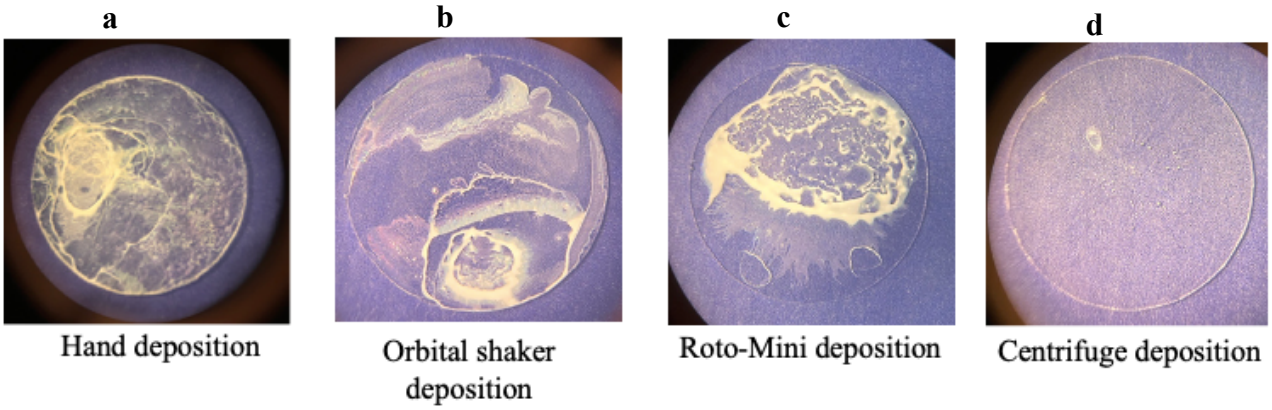

Figure 11. Resultant glass cover slips of various polystyrene sphere deposition methods.

a more uniform deposition and the iridescent colour of the sensor chip suggested an even monolayer distribution of the polystyrene spheres.

To be confident that the substrate has monolayer coverage of spheres, the surface of the centrifuge deposition substrate (Fig 11d) was investigated with a scanning electron microscope. Fig A1 shows that the centrifuge method achieved the best single layer deposition of the polystyrene spheres, so this deposition method was used for all polystyrene depositions in this research.

3.1.2 Polystyrene sphere suspension studies

Not only is it important for the polystyrene spheres to be present in a monolayer, but also the area covered by the spheres must be maximized to produce a strong LSPR signal. The distribution of the polystyrene spheres on the surface of the glass cover slip is highly dependent on the solution that the spheres are suspended in. Four solutions (shown in Table 1, Section 2.2.2)

were explored to determine which would result in an optimal coverage of the polystyrene spheres in a monolayer. The deposition solutions tested were a 1:1 % v/v mixtures of the spheres as

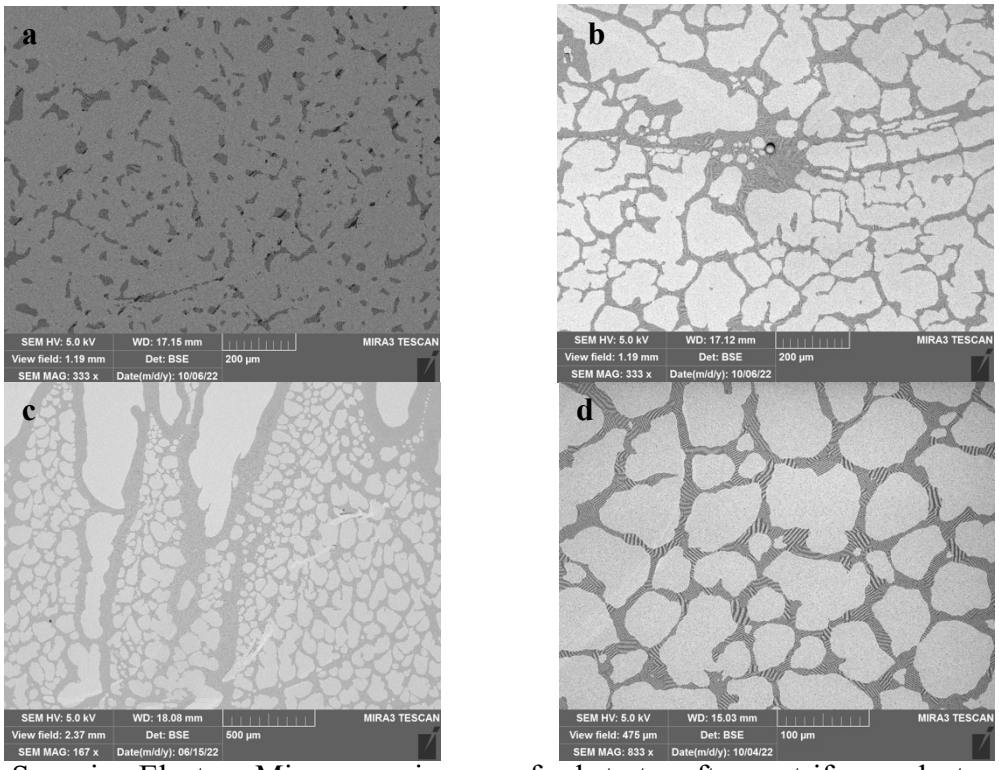

Figure 12. Scanning Electron Microscope images of substrates after centrifuge polystyrene depositions: a) with ethylene glycol solution, b) with sphere solution as purchased, c) with methanol, d) with surfactant solution.

purchased with one of the following chemicals: methanol, ethylene glycol, spheres as purchased (in water) or a surfactant solution (TX-100 : methanol, 1:400 v/v). Figure 12 shows the distribution of the polystyrene spheres on the surface of the glass cover slip for each solution.

Ethylene glycol was used to assess how increasing the viscosity of the sphere solution would influence sphere deposition. The resulting substrates from this deposition solution had sparsely distributed multilayers of the polystyrene spheres with a poor percent coverage of 11% (Fig 12a). These results were undesirable, and the use of this solution was discontinued.

Depositions with the sphere solution as purchased were performed with the prediction that a higher concentration of the spheres in solution would result in a better coverage. This deposition

did produce a better coverage (25%), however multi-layers were an issue particularly around some larger spheres which were a manufacturing defect (Fig 12b, Fig A2). The clumped spheres do not exhibit the optical properties needed for LSPR and so they would interfere with the intensity and reproducibility of the LSPR signal. As such, deposition using the sphere solution only was also discontinued.

Depositions with methanol had a decent coverage, however the deposition was not uniform across the surface as exhibited areas with no spheres (Fig 12c). Additionally, the three solutions discussed so far did not give reproducible sphere distribution and percent coverages with each trial.

The surfactant solution was explored due to their ability to increase wettability of the sphere suspension as mentioned in section 2.2.2. Sphere depositions using the surfactant solution (Fig 12d) gave uniform deposition across the surface of the glass slide and had an average coverage of 17.68% ± 2.72% calculated from 4 trials (Table A1). Additionally, the surfactant solution gave reproducedable coverage making it more consistent than the other solutions investigated. Moving forward, the polystyrene sphere depositions were performed with the surfactant solution as it was found to provide optimal sphere distribution.

3.1.3 Polystyrene sphere concentration studies

Although the depositions with the sphere solution as purchased did not give the desired sphere monolayer, it presented a decent coverage as mentioned in 3.1.2. This led to investigating how the concentration of spheres in the deposition solution can affect the coverage of the spheres on the glass coverslip. Tests were carried out to determine if increasing the ratio of sphere solution : surfactant solution (% v/v) from 1:1 to 3:1 (Table A1) would improve the coverage of the spheres on the substrate. The percent coverage of the spheres was measured on a smaller portion of the

substrate and because the deposition was found to be uniform across the surface (Fig 13d), it was assumed that the percent coverage is the same on the rest of the substate.

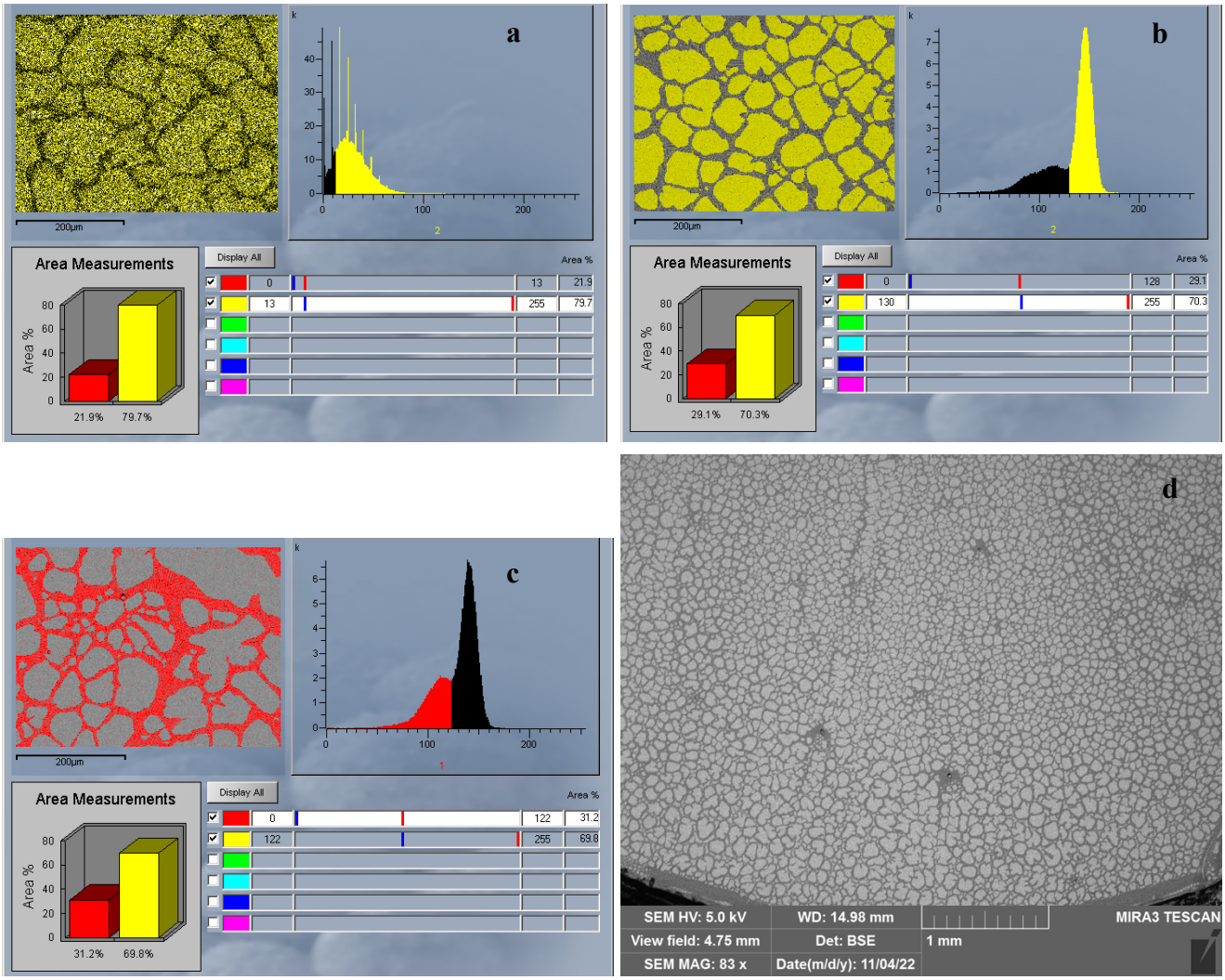

Figure 13. Percent coverages sphere: surfactant solutions of varying ratios a) 1:1, b) 2:1, c) 3:1. d) SEM image of a larger area of the substrate showing uniform deposition across surface. The histogram beneath the BSE image shows the percentages of the contrasting colours of the spheres and the bare glass which is representative of percent sphere coverage. The red indicates areas where the polystyrene spheres are deposited and the yellow indicated unoccupied area.

Figures 13a , 13b and 13c show screenshots of windows of the INCA® software used to calculate the percent sphere coverage. The coloured SEM image on the top left of each screenshot is a back scattered electron (BSE) image of the section of the substrate measured for percent sphere coverage. The SEM image was taken using a BSE detector as it gives a better contrast since the

software uses pixels of the SEM image to make its measurements. The histogram beneath the BSE image shows the percentages of the contrasting colours of the spheres and the bare glass which is representative of percent sphere coverage. For example, in Fig 13c on the BSE the red is indicating the area where the polystyrene spheres are deposited (red bar on histogram) and the grey is unoccupied area (yellow bar on histogram).

Depositions of 5 samples of 1:1 solution gave an average coverage of 17.68% ± 2.72%. The 2:1 solution deposition produced an average percent coverage of 34.37% ± 7.13% for 8 samples from different batches made on different days (Table A1). The %RSD for this data was 20.74% which shows that the percent coverage data for the 2:1 deposition is statistically uniform as there is insignificant variation between the data collected and so this deposition method is reproducible. The 3:1 deposition averaged 28.74 % ± 4.44% for 5 samples from different batches (Figure 13, Table A1). Although the 3:1 has a lower sphere coverage compared to the 2:1, the variance of the data is lower (3:1 exhibited 15.45 %RSD, Table A1). The evidence shows 3:1 gave better reproducibility whereas the 2:1 gave better percent coverage which partially satisfied the prediction about increasing the sphere concentration to improve percent sphere coverage.

Moving forward polystyrene spheres were deposited onto the glass cover slips by centrifugation with either 2:1 or 3:1 (sphere : surfactant solution) sphere deposition solution. The optimum volume of the sphere/surfactant solution was determined to be 15 μL for the 18 mm diameter cover slips and 7 μL for the 12 mm diameter cover slips.

3.2 Building a plasmonically active sensor base

Metal nanoparticle structures are known to be plasmonically active and can produce an LSPR extinction spectrum[19,24, 25, 30] . In this research, hexagonal close packed (HCP) monolayer

masks, gold nanoparticles (AuNP), and thin film over nanosphere (AgFONs) sensor chips were fabricated and compared to determine which produced the strongest LSPR signal.

3.2.1 Hexagonal-close-packed (HCP) monolayer studies

The polystyrene spheres deposited by the optimized method discussed in 3.1.3 function as a sacrificial mask for making HCP substrates. A thin layer of silver was deposited on the polystyrene spheres which were then dissolved. Several chemicals were tested to determine which

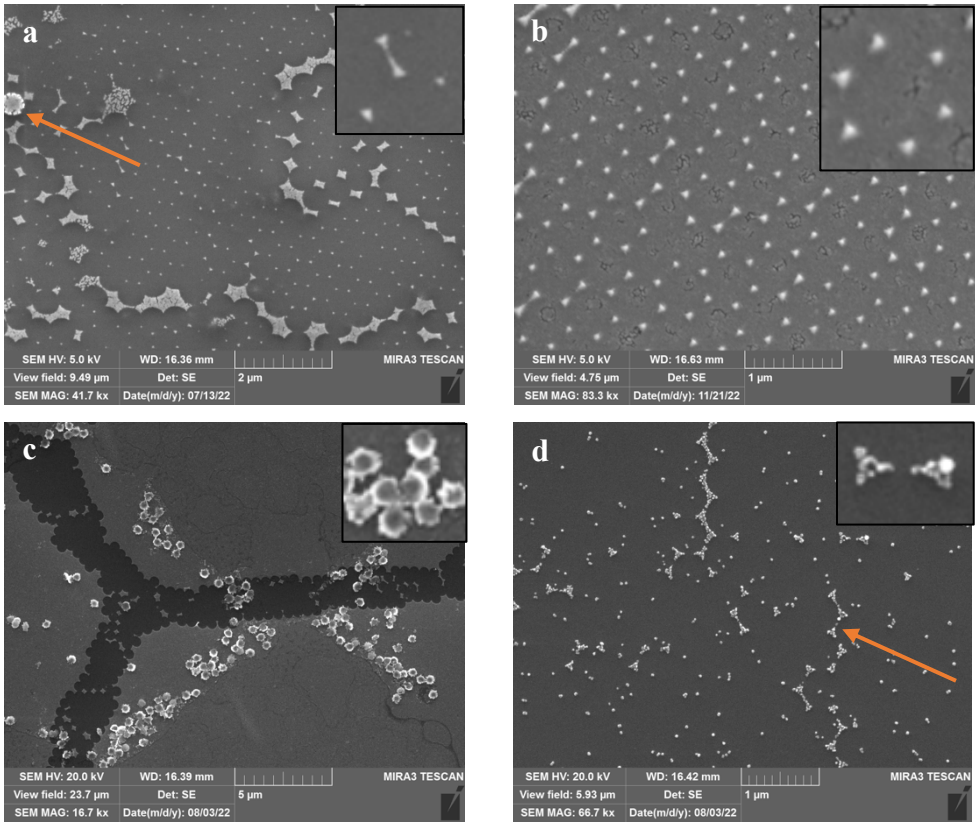

Figure 14. SEM images of substrates after dissolving the polystyrene spheres in a) toluene for 1 minute orange arrow shows undissolved polystyrene spheres, b) toluene for 1.5 min, c) ethanol for 1.5 min, and d) dichloromethane for 1.5 min, orange arrow points to degraded bowtie features. An enlarged insert of the plasmonic metal features are shown on the top right of each figure.

would efficiently remove the spheres and produce the desired silver structures. Fig 14a shows the resulting features from dissolution in toluene after 1 minute and Fig 14b shows the structures after 1.5 minutes. The extra 30 seconds of sonication in the toluene made a difference as all the spheres

were effectively dissolved. Fig 14c shows that the ethanol was ineffective at dissolving all of the polystyrene spheres. The dichloromethane effectively dissolved the spheres however, it was deteriorating the desired triangles/bow-tie features (orange arrow on Fig 14d). The toluene showed the best removal of spheres and produced clear cut triangle/bow-tie features (Fig 14a,b). Moving forward, the hexagonal-close-packed (HCP) monolayer was achieved by dissolving the spheres in toluene for 1.5 min.

The HCP substrates were tested to determine their LSPR signal intensity. Varying thicknesses of silver (20 nm, 30 nm, 50 nm, and 100 nm) were deposited on the substrates to ascertain the optimum silver thickness that would give the best LSPR signal. All LSPR experiments were performed using the Ocean Optics UV-VIS NIR spectrometer equipped with a USB2000+ Ocean Optics linear CCD array detector. Measurements were taken in transmission mode in the dark, and the data acquired was baseline corrected.

Hexagonal close packed (HCP) monolayers of nano-triangular/bowtie features have been successfully used as an LSPR sensing platform for diagnosis of various types of cancers [1,2]. In this research the optimized HCP masks were successfully fabricated uniformly on glass cover slips (Fig 14b) however, they did not manage to produce an LSPR peak which is expected to be around ~600nm for silver [13,19]. Figure 15 shows the LSPR spectra of the substrates of varying silver thicknesses. The sharp peak at ~670 nm was credited to an artifact of the instrument. The peaks at 350 nm and ~580 nm could not be assigned. A control study was conducted to determine if the signal is being produced by the silver metal itself (15 nm of silver deposited on a glass cover slip) or the glass. The glass is transparent and so the LSPR extinction spectra presented a plateaued peak at 100% transmission (black spectral line Fig A2). It was also found that the signal for the silver only substrate (blue spectral line Fig A2) is identical to that of the HCP substrate (red spectral line

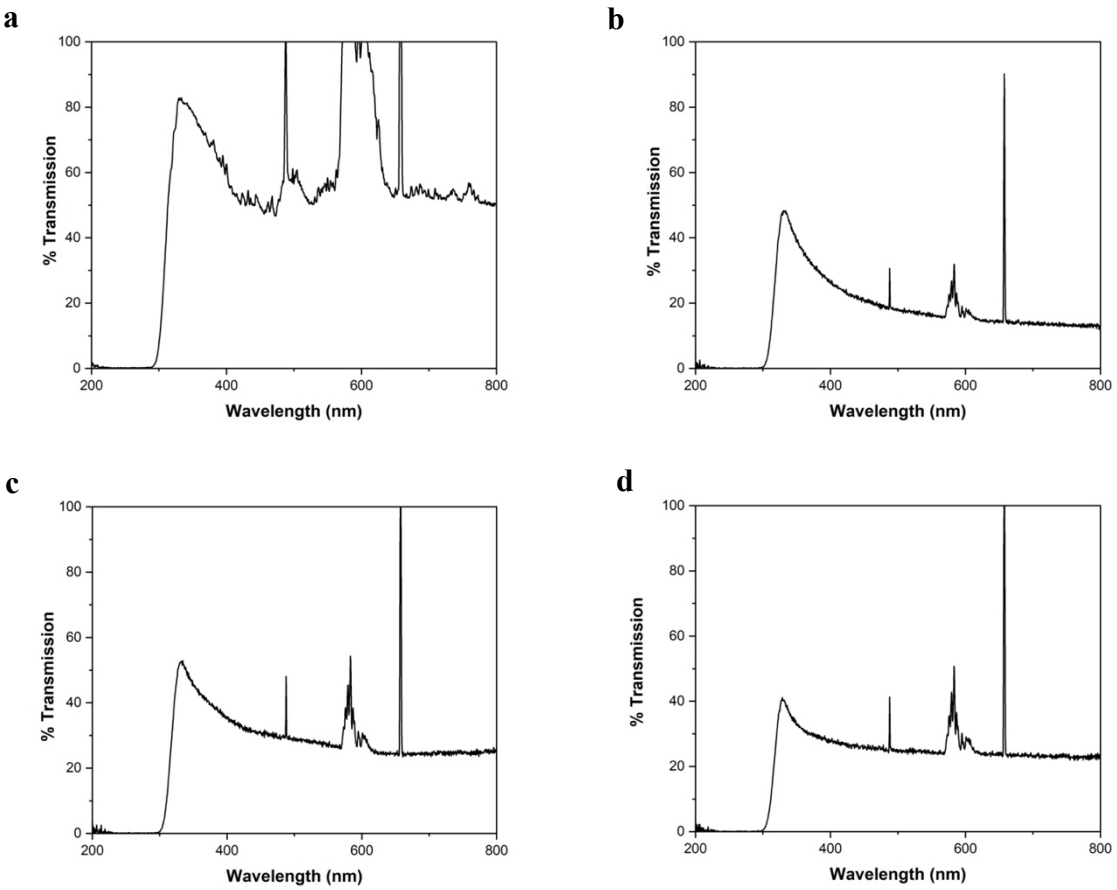

Figure 15. LSPR spectra of hexagonal close packed monolayer substrates of varying thicknesses of silver. a) 20 nm, b) 30 nm c) 50 nm, d) 100 nm

Fig A2) except it is lower in %transmission intensity. This means that the signal observed in Fig15 by the HCP masks is not from the plasmonic properties of the bowtie features. Instead, the signal observed is from the silver itself blocking some of the light being transmitted through the sample. The reason behind the lack of an LSPR peak could be that the nanoparticle features were not dense enough to produce a measurable LSPR signal using this instrument[13].

3.2.2 Gold nanoparticles (AuNP) sensor studies

Gold nanoparticles (AuNP) were investigated as a substitute for the failed HCP masks since they are plasmonically active[14]. The AuNP were investigated because it was predicted that the coverage of the AuNP on the surface of the APTMS modified substrate would be greater than that of the

HCP masks. 1% 3-aminopropyl-triethoxysilane was used to modify the surface of the glass cover slip to allow gold nanoparticles to bind to the glass surface[30]. The cover slips were incubated in a suspension of AuNP solution for 16- and 24- hours to allow for maximum attachment of the AuNP.

The resulting AuNP substrates appeared to have a superior coverage on the surface of the sensor (Figure A1) when visually compared to the HCP masks (the percent coverage of the AuNP substrates was not determined). The resultant substrates were tested for their LSPR signal intensity using the UV-VIS NIR spectrometer in transmission mode. The transmission values were transformed to absorbance values using the equation below where A is the absorbance/extinction and T is the transmission value:

$$A = -\log T$$

The AuNP substrates produced a weak LSPR peak between 500 nm – 550 nm but the signals were too weak to proceed with functionalizing the sensor base (Figure 16). A longer incubation time in AuNP solution (24 hours vs 16 hours) was explored to allow for more time for the AuNP to bind to the surface of the glass coverslip to increase the area occupied by the nanoparticles. This had virtually no effect on the signal intensity of the LSPR peak (Fig 16a and Fig 16b). As mentioned earlier, the AuNP were expected to produce a weaker LSPR signal however, the extent of the signal reduction experienced in this experiment was greater than expected and could be due to the size of the nanoparticles. LSPR is highly dependent upon the size and shape of nanostructures[18] and so the size of the AuNP synthesized in this research might not have been the optimum size required to produce a strong enough LSPR signal.

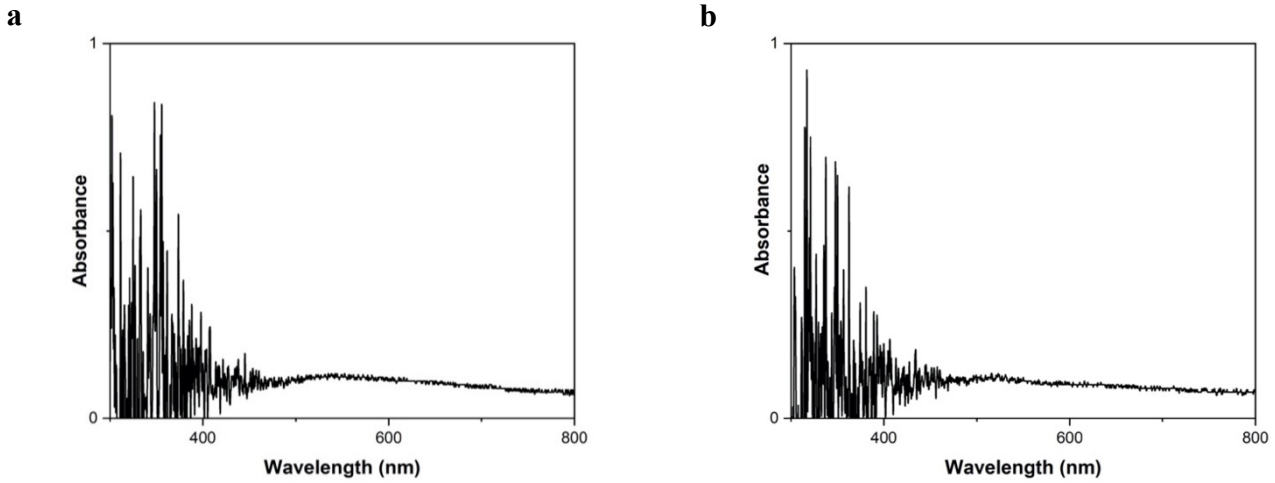

Figure 16. LSPR spectra of gold nanoparticle substrates. a) 16-hour incubation in AuNP solution, b) 24-hour incubation in AuNP solution

3.2.3 Silver film over nanosphere (AgFON) studies

As a last final attempt to produce a functional sensor, silver film over nanospheres (AgFON) were studied to determine their LSPR activity. The AgFONs were fashioned as described in section 2.4. The LSPR measurements for this substrate type were taken in reflectance mode because the thicker amount of silver deposited does not allow light to pass through the substrate so transmission measurements would be ineffective.

Figure 17a shows a plot of overlayed LSPR spectra from different spots on the same AgFON substrate. A strong LSPR (λ_{max}) peak was observed at 600 nm. The sharp peak at ~660 nm is an instrument artifact and was ignored. The signal intensity of the LSPR was saturating the detector (reflectance intensities past 100%) so this was controlled by setting the integration time of the UV-VIS NIR spectrometer to 65 ms - 68 ms on the Ocean Optics software to standardize measurements going forward.

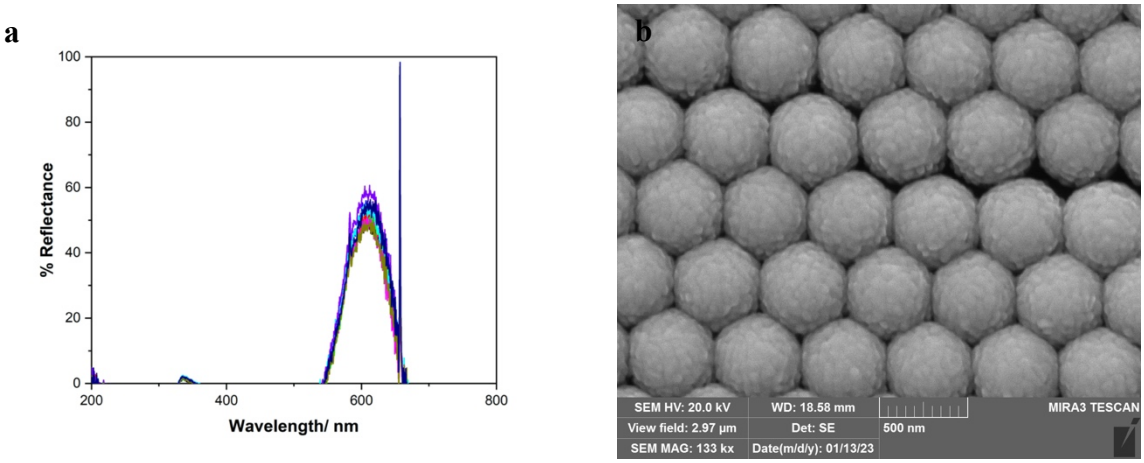

Figure17. a) Overlayed LSPR spectra of AgFON, b) SEMimage of the AgFONs

The signal intensity reported in % reflectance for the sensor was uniform across the surface of the sensor as exhibited by the statistically favourable %RSD values which were all below 20 %RSD (Table A1). The %RSD (coefficient of variance) values were calculated based off several random spots on the sensor. The signal uniformity and intensity were also reproducible between different batches of AgFONs (Table A1). As a result, it can be concluded that the signal is uniform across the surface of the sensor and so measurements can be taken at a random spot and produce a uniform signal. This is useful as it reduces the time needed for measurements to be taken as one can be confident that the signal obtained is optimal. This allows for application of this sensor in a fast-paced environment. A plasmonically active sensor base has been successfully fabricated and fulfilled the first objective of the thesis.

3.3 LSPR Sensing on Aptasensor

As previously discussed, localised surface plasmon resonance (LSPR) is sensitive to the changes that occur in the dielectric environment near the nanometal surface [18]. As a result, LSPR can be used to transform molecular interactions into quantifiable signals which are experienced as

LSPR (λ_{max}) peak shifts[13]. Cited literature reports shifts in the LSPR peak wavelength at each stage of modification of the sensor [13, 14,19]. Correspondingly, LSPR measurements were taken at each step of assembling the aptasensor to determine the changes that would be observed in the LSPR spectrum. Taking measurements at each step of the sensor assembly provides confidence that changes experienced between the LSPR spectra of the aptasensor prior to and after introduction of the analyte is solely due to cTnI interaction with the aptamer. LSPR measurements on the aptasensor were performed with the UV-VIS NIR spectrometer in reflectance mode in the dark. The sensor was functionalized in the following order: the aptamer was first covalently assembled onto the AgFON substrate, then backfilling thiols were allowed to self-assemble and fill in the gaps to prevent non-specific binding which could result in false positives. Each % reflectance reported is the average of a minimum of six spots on the same sample ± standard deviation (see appendix for raw data, Tables A1- A8).

Initial LSPR studies on the aptasensor were performed without the aptamer because the aptamer solution was causing delamination of the silver on the AgFON substrates. Control studies were performed where the AgFONs were incubated for an hour in each solution used in the whole experimental process to determine which was causing the delamination. The TCEP reducing agent for the aptamer was isolated as the cause of delamination, so the aptamer was not used except in one experiment.

A control study was conducted to monitor the LSPR peak shift experienced when the cTnI protein is deposited on a bare unmodified AgFON substate. A measurement was taken on the bare AgFON (red spectrum Fig 18a) then another after cTnI deposition (black spectrum Fig 18a).

Adding the cTnI protein onto the bare AgFON resulted in a peak shift to the blue region (shorter wavelengths) from 600 nm to 520 nm (Figure 18a).

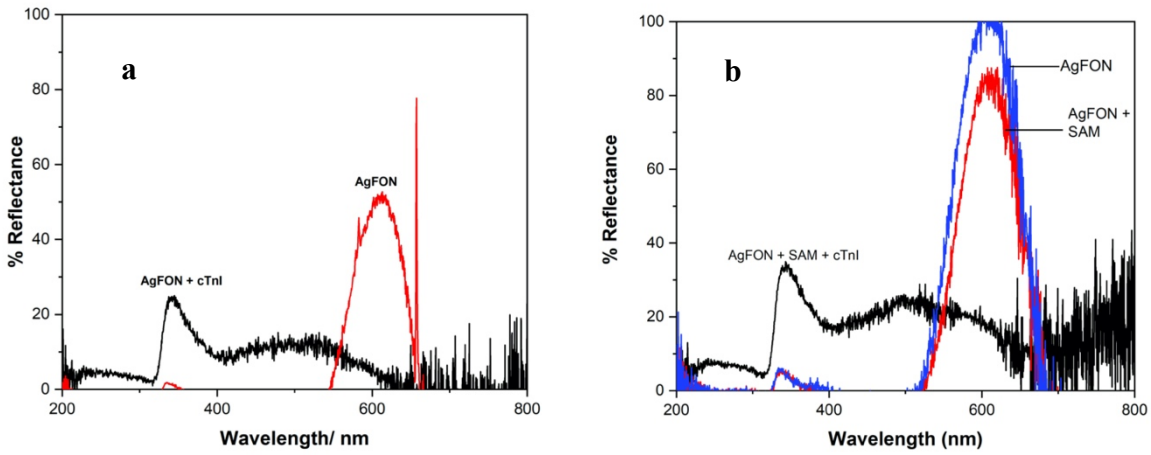

Figure 18. Overlay of LSPR spectra of **a)** bare AgFON (red), AGFON + cTnI (black) and **b)** bare AgFON (blue), AgFON modified by self-assembled monolayer (SAM) of thiol back filling agents (red), and SAM modified AgFON + cTnI (black)

A study was carried out where LSPR measurements were taken on a AgFON modified with the thiol backfilling agents and the protein (Figure 18b). An LSPR measurement was taken at each step of modifying the AgFON and the overlays of the LSPR spectra are shown in Figure 18b. Addition of the backfilling agents did not cause a shift in LSPR peak wavelength, instead the peak intensity decreased from ~100% reflectance to 82% ± 4% reflectance (Figure 18b, Table A4). This decrease in reflectance could be related to the thiol molecules on the surface which are potentially absorbing some of the incident light thus reducing the amount reflected.

Adding the protein sample onto the thiol modified sensor caused a drastic decrease in % reflectance from 82% to 21 % and a 117 nm shift in the wavelength to the blue region (Figure 18b, Table A5). The decrease in % reflectance is due to the molecules present on the analyte reducing the amount of light reflected. The shift in wavelength of the LSPR peak in this case indicates the presence of a large biomolecule as expected. The resultant LSPR peak produced after addition of

cTnI had the same wavelength on both the unmodified and thiol modified AgFON substrates (480 nm- 490 nm, black spectrum Fig 18a unmodified AgFON and black spectrum Fig 18b AgFON modified with thiols). Additionally, the once negligeable peak at 498 nm rose to a % reflectance that averaged 21.5 % ± 2.8% (Table A8). An increase in intensity of a peak upon addition of analyte is something not observed in cited literature and so the cause of this result is inconclusive.

LSPR measurements were attempted on the AgFON sensor modified with the aptamer. To

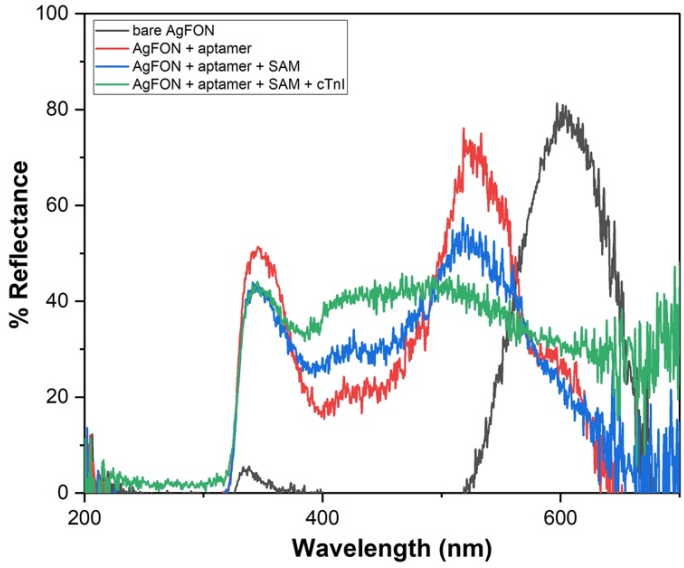

Figure 19. Overlay of LSPR spectra taken at each stage of the sensor assembly, AgFON only (black), AgFON and aptamer (red), AgFON + aptamer + thiol backfilling agents (blue) and AgFON aptamer + thiol backfilling agents + cardiac troponin I (cTnI) (green).

minimize silver delamination, 10 μL of each of the thiol backfilling agents were drop casted onto the aptamer modified sensor instead of immersing the sensor in the thiol solution. The drop casted AgFONs were allowed to stand at room temperature for 2 hours with 12-MDA and 30 min with cysteamine (consistent with incubation times in section 2.3.5). No rinsing steps were done in order to avoid washing away the silver. This study was done to determine the effect that the aptamer would have on the LSPR peak so that the shifts caused by aptamer interaction with cTnI can be

reported accurately and not be overstated. Figure 19 shows the overlayed spectra of each stage of the sensor assembly namely bare AgFON , AgFON + aptamer, AgFON + aptamer + thiol backfilling agents and finally AgFON aptamer + thiol backfilling agents + cardiac troponin I (cTnI). A blue shift from 600 nm to 522 nm is experienced upon modifying the AgFON with the aptamer (red spectral line Fig 19). Adding the thiol backfilling agents resulted in a decrease in % reflectance from 49% ± 4% to 37% ± 8% (blue spectral line Fig19, Table A7). The LSPR peak of the aptasensor prior to introducing the sample was at 522 nm and this peak shifted to 480 nm – 490 nm after addition of the cTnI sample (green spectral line Fig 19). The modification of the surface during sensor assembly causes a change in the local refractive index of the sensor and this causes a shift in the LSPR peak wavelength [19]. The results obtained for the LSPR measurements on the aptasensor were not entirely in agreement with results experienced in similar LSPR sensing platforms from the literature. While the shift in the LSPR peak was a common factor, the direction of the peak shifts in this experiment was to the blue region which is opposite of the red shift reported in most of the literature[13, 14, 18,19] . It was of interest to determine the cause of the blue shift instead of the red shift in these results.

Blue shifts are typically associated with change in shape or reduction in size of nanostructures[31], small molecule binding[18], or change in surrounding medium[31]. However, these parameters were kept constant in this research therefore an explanation for the blueshift experienced in this work is inconclusive. This does not take away from the functionality of the sensor as it still communicates the biomolecular interactions occurring at the surface of the sensor. Further experiments can be performed to determine the spectral shifts experienced with various concentrations of cTnI and determine the limit of detection of the aptasensor (i.e., the smallest concentration of cTnI that can elicit a shift in LSPR peak).

Future experiments can be carried out to determine if the protein is binding to the aptamer and determine the LSPR spectrum that this interaction would produce. This could not be accomplished in this thesis work because the delamination of the silver prevented the practice of a rinsing step which would have otherwise removed unbound protein and enabled us to see the LSPR spectrum produced by aptamer bound protein. LSPR spectrum with cTnI sample in this work (green spectrum, Fig 19) is not representative of the protein that is bound to the aptamer because the excess was not washed off. Accordingly, a new reducing agent for the aptamer that does not delaminate the sensor is required for future research to be successful.

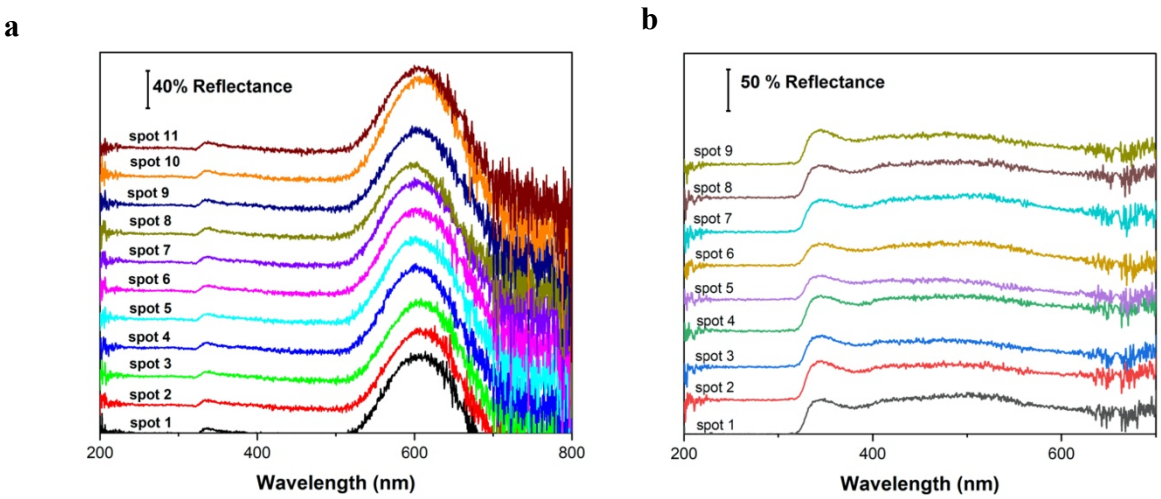

Figure 20. Stacked LSPR spectra of several spots on a) bare AgFONs and b) functionalized sensor + cardiac troponin protein.

Uniformity and reproducibility of the signal across the surface of the aptasensor was determined by taking measurements on a minimum of 6 spots then averaging the percent reflectance and reporting the data with standard deviations as well as coefficients of variables. The resulting LSPR spectra were overlayed. Figure 20a shows the stacked spectra of several spots of a bare AgFON substrate and Figure 20b shows the stacked of spectra several spots of the fully functionalized sensor with the cTnI sample (same sample as the green spectral line Fig 19). The

plot for the bare AgFON averaged a % reflectance of 82% ± 7% and had a coefficient of variance of 8% RSD (Table A2). The plot for the functionalized sensor plus the cTnI sample had an average of 21% ± 3% reflectance and the coefficient of variance is reported to be 13 %RSD (Table A8). The low standard deviations and coefficients of variables for the spots on each sample reported in the data (Tables A1-A8) provide statistical evidence that suggest that the signal produced across the surface of the sensor is uniform even after modification with the ternary monolayer. The aptasensor fashioned in this thesis work is reported to produce a uniform and reproducible LSPR signal across the surface of the sensor.

3.4 Limitations of study

A major drawback in the study was the delamination of the silver caused by the reducing agent. This prevented accurate evaluation of the spectral shift ($\Delta\ \lambda_{max}$) experienced when the aptamer binds cTnI protein. The data reported for the LSPR peak shift of the ternary monolayer after addition of cTnI reported is overstated for reasons discussed in section 3.3. The small sample size for the LSPR measurements of the different ternary monolayer components is because the study focused on building the aptasensor since several methods failed to produce the LSPR functionality. More samples would need to be measured to report consistency of spectral shift data of the ternary monolayer components with a higher level of confidence. Taking away these limitations, this research work produced an optimized nanosphere lithography method which was used to fabricate an LSPR sensor base that could detect adsorption of biomolecules on its surface, as well as display analytical data of the bimolecular interaction of the aptamer with the protein cTnI.

CHAPTER 4: CONCLUSIONS

The main objective of this thesis work was to develop an aptasensor for the detection of cardiac troponin I (cTnI, the golden standard biomarker for acute myocardial infarction) using localised surface plasmon resonance (LSPR) as a sensing platform. An optimized plasmonically active sensor base was successfully fashioned by an optimized nanosphere lithography method. Centrifugal deposition of a mixture of polystyrene spheres and surfactant solution were the optimal parameters to obtain maximum coverage and uniform distribution of the polystyrene spheres. A 2:1 ratio of the sphere solution : surfactant solution produced substrates with an average of 34.37% ± 7.13 % coverage across the surface and 3:1 ratio produced 28.74 % ± 4.44% sphere coverage.

It was determined that silver film over nanosphere (AgFON) substrates functioned the best to produce strong, reproducible LSPR peaks. The signal across the AgFONs was significantly uniform as evidenced by the coefficient of variance values of the % reflectance of the sensors which were below <20%RSD. The low RSD suggests that the reflectance values did not differ significantly for variable spots on the sensor (Tables A1-A8). LSPR measurements of the AgFON prior to and after the addition of cTnI and aptamer showed a blueshift in the LSPR peak. A blueshift of the LSPR peak was observed instead of the commonly known redshift. The reason behind this observation was inconclusive given the reasons provided by cited literature were inapplicable to the conditions of this research. Regrettably, the reducing agent used for reducing the aptamer caused delamination of the silver on the AgFONs so the exact LSPR peak produced by the interaction of the aptamer with cTnI could not be determined. This research served as a proof of concept that an LSPR based aptasensor can be used for cTnI detection and has potential for application in a clinical setting. Further investigations for precise quantification of the dynamic linear range, limit of detection and large-scale production of the sensor are worth pursuing.

CHAPTER 5: FUTURE WORKS

The next crucial step for this research would be to find a replacement reducing agent for the aptamer that does not delaminate the sensor. It is worth noting that sulphur rich chemicals must be avoided for the aptamer reducing agent replacement due to the strong Ag-S bonds which could result in incorrect bonding of the aptamer to the sensor surface and reduce sensor functionality. An option could be using an adhesion layer such as Titanium or Aluminium between the glass and the silver which could prevent the delamination of the silver even when using TCEP. A standard calibration curve could be determined using varying concentrations of the cTnI plotted against the peak shift ($\Delta\ \lambda\max$) that each sample causes. The limit of detection of the sensor can also be determined to assess its potential for use in detecting physiological concentrations of the cTnI in both patient and non-patient blood samples.

Additionally, the sensor could be tested for selectivity by introducing a sample with other cardiac troponin proteins. This study can be extended to identify the interference matrices in a blood sample to assess whether the blood sample requires any pre-treatment (such as extracting plasm). Lastly, this research presents opportunities of reducing the cost of AMI diagnosis and can even be evaluated for reusability to reduce waste. Since the aptamer binds to the protein by strong non-covalent forces, it could be possible to incubate the used sensor in a high/low pH or a strong ionic strength solution to liberate the aptamer. Control studies would need to be carried out to determine if any damage is caused to the aptamer, the number of times the sensor can be reused, and what the percent performance of the recycled sensor is compared to a freshly prepared one.

CHAPTER 6: REFERENCES

1. Minatoguchi, S. *Cardioprotection Against Acute Myocardial Infarction*. Springer Verlag, Singapore, **2021**.
2. Thygesen, K.; Alpert, J. S.; Jaffe, A. S.; Simoons, M. L.; Chaitman, B. R.; White, H. D. Third Universal Definition of Myocardial Infarction. *Nature Reviews Cardiology* **2012**, *9* (11), 620–633.
3. Mehta, L. S.; Beckie, T. M.; DeVon, H. A.; Grines, C. L.; Krumholz, H. M.; Johnson, M. N.; Lindley, K. J.; Vaccarino, V.; Wang, T. Y.; Watson, K. E.; Wenger, N. K. Acute Myocardial Infarction in Women. *Circulation* **2016**, *133* (9), 916–947.
4. American Heart Association, Council on Epidemiology and Prevention Statistics Committee and Stroke Statistics Subcommittee. Heart Disease and Stroke Statistics—2018 Update: A Report from the American Heart Association. *Circulation* **2018**, *137* (12).
5. *Report from the Canadian Chronic Disease Surveillance System: Heart Disease in Canada, 2018*; Public Health Agency of Canada: Ottawa, ON, 2018. ISBN 978-0-660-24021-3.
6. Ko, D. T.; Ahmed, T.; et. al. Austin, P. C.; Cantor, W. J.; Dorian, P.; Goldfarb, M.; Gong, Y.; Graham, M. M.; Gu, J.; Hawkins, N. M.; Huynh, T.; Humphries, K. H.; Koh, M.; Lamarche, Y.; Lambert, L. J.; Lawler, P. R.; Légaré, J.-F.; Ly, H. Q.; Qiu, F.; Quraishi, A. ur; So, D. Y.; Welsh, R. C.; Wijeysundera, H. C.; Wong, G.; Yan, A. T.; Gurevich, Y. Development of Acute Myocardial Infarction Mortality and Readmission Models for Public Reporting on Hospital Performance in Canada. *CJC Open* **2021**, 3 (8), 1051–1059.
7. Chung, S.-C.; Gedeborg, R.; Nicholas, O.; James, S.; Jeppsson, A.; Wolfe, C.; Heuschmann, P.; Wallentin, L.; Deanfield, J.; Timmis, A.; Jernberg, T.; Hemingway, H.

Acute Myocardial Infarction: A Comparison of Short-Term Survival in National Outcome Registries in Sweden and the UK. *The Lancet* **2014**, *383* (9925), 1305–1312.

8. Katrukha, I. A. Human Cardiac Troponin Complex. Structure and Functions. *Biochemistry (Moscow)* **2013**, *78* (13), 1447–1465.
9. Cheng, Y.; Regnier, M. Cardiac Troponin Structure-Function and the Influence of Hypertrophic Cardiomyopathy Associated Mutations on Modulation of Contractility. *Archives of Biochemistry and Biophysics* **2016**, *601*, 11–21.
10. Babuin, L.; Jaffe, A. S. Troponin: The Biomarker of Choice for the Detection of Cardiac Injury. *Canadian Medical Association Journal* **2005**, 1191–1202.
11. Jo, H.; Gu, H.; Jeon, W.; Youn, H.; Her, J.; Kim, S.-K.; Lee, J.; Shin, J. H.; Ban,C. Electrochemical Aptasensor of Cardiac Troponin I for the Early Diagnosis of Acute Myocardial Infarction. *Anal. Chem*. **2015**, 87(19), 9869–9875.
12. Nezami, A.; Dehghani, S.; Nosrati, R.; Eskandari, N.; Taghdisi, S. M.; Karimi, G. Nanomaterial-Based Biosensors and Immunosensors for Quantitative Determination of Cardiac Troponins. *Journal of Pharmaceutical and Biomedical Analysis* **2018**, *159*, 425–436.
13. Xi, M.; Zhao, Q.; Duan, R.; Yuan, J.; Quan, Y.; Yang, H. A Reusable Localized Surface Plasmon Resonance Biosensor for Quantitative Detection of Serum Squamous Cell Carcinoma Antigen in Cervical Cancer Patients Based on Silver Nanoparticles Array. *International Journal of Nanomedicine* **2014**, 1097.
14. Zhou, W. A Label-Free Biosensor Based on Silver Nanoparticles Array for Clinical Detection of Serum p53 in Head and Neck Squamous Cell Carcinoma. *International Journal of Nanomedicine* **2011**, 381.

15. Chen, A., and Yang, S. Replacing antibodies with aptamers in lateral flow immunoassay. *Biosensors and Bioelectronics* **2015,** *71*, 230–242.

16. Kong, T.; Su, R.; Zhang, B.; Zhang, Q.; Cheng, G. CMOS-Compatible, Label-Free Silicon-Nanowire Biosensors to Detect Cardiac Troponin I for Acute Myocardial Infarction Diagnosis. *Biosensors and Bioelectronics* **2012**, *34* (1), 267–272.

17. Tombelli, S.; Minunni, M.; Mascini, M. Analytical Applications of Aptamers. *Biosens. Bioelectron.* **2005**, 20(12), 2424–2434.

18. Willets, K. A.; Van Duyne, R. P. Localized Surface Plasmon Resonance Spectroscopy and Sensing. *Annual Review of Physical Chemistry* **2007**, *58* (1), 267–297.

19. Zhu, S.; Li, F.; Du, C.; Fu, Y. A Localized Surface Plasmon Resonance Nanosensor Based on Rhombic AG Nanoparticle Array. *Sensors and Actuators B: Chemical* **2008**, 134 (1), 193–198.

20. Development of an Electrochemical Surface-Enhanced Raman Spectroscopy Aptasensor for the Early Detection of Acute Myocardial Infarction By: Sam Michael Julien

21. Wain, A. J.; O'Connell, M. A. Advances in Surface-Enhanced Vibrational Spectroscopy at Electrochemical Interfaces. *Adv. Phys. X* **2017**, *2* (1), 188–209.

22. Masson, J.-F. Portable and Field-Deployed Surface Plasmon Resonance and Plasmonic Sensors. *The Analyst* **2020**, *145* (11), 3776–3800.

23. Haes, A. J.; Zou, S.; Schatz, G. C.; Van Duyne, R. P. A Nanoscale Optical Biosensor: the Long Range Distance Dependence of the Localized Surface Plasmon Resonance of Noble Metal Nanoparticles. *The Journal of Physical Chemistry B* **2003**, *108* (1), 109–116.

24. Lee, J.; Zhang, Q.; Park, S.; Choe, A.; Fan, Z.; Ko, H. Particle–Film Plasmons on Periodic Silver Film over Nanosphere (AgFON): A Hybrid Plasmonic Nanoarchitecture for Surface-Enhanced Raman Spectroscopy. *ACS Applied Materials & Interfaces* **2015**, *8* (1), 634–642.
25. Hulteen, J. C.; Treichel, D. A.; Smith, M. T.; Duval, M. L.; Jensen, T. R.; Van Duyne, R. P. Nanosphere Lithography: Size-Tunable Silver Nanoparticle and Surface Cluster Arrays. *The Journal of Physical Chemistry B* **1999**, *103* (19), 3854–3863.
26. Karaballi, R.; Nel, A.; Krishnan, S.; Blackburn, J.; Brosseau, C. Development of an Electrochemical Surface-Enhanced Raman Spectroscopy (EC-SERS) Aptasensor for Direct Detection of DNA Hybridization. *Phys. Chem. Chem. Phys.* **2015**, *17* (33), 21356–21363.
27. Reduction for Oligonucleotides with Thiol Modifications, 2020.
28. Lim, G.; Hwang, H. J.; Kim, J. H. Protected Immobilization of Taq DNA Polymerase by Active Site Masking on Self-Assembled Monolayers of ω-Functionalized Thiols. *Analytical Biochemistry* **2011**, *419* (2), 205–210.
29. Ji, X.; Song, X.; Li, J.; Bai, Y.; Yang, W.; Peng, X. Size Control of Gold Nanocrystals in Citrate Reduction: Third Role of Citrate. *Journal of the American Chemical Society* **2007**, *129* (45), 13939–13948.
30. Oh, S. Y.; Heo, N. S.; Bajpai, V. K.; Jang, S.-C.; Ok, G.; Cho, Y.; Huh, Y. S. Development of a Cuvette-Based LSPR Sensor Chip Using a Plasmonically Active Transparent Strip. *Frontiers in Bioengineering and Biotechnology* **2019**, *7*.

31. Sahu, A. K.; Das, A.; Ghosh, A.; Raj, S. Understanding Blue Shift of the Longitudinal Surface Plasmon Resonance during Growth of Gold Nanorods. *Nano Express* **2021**, *2* (1), 010009.

CHAPTER 7: APPENDIX

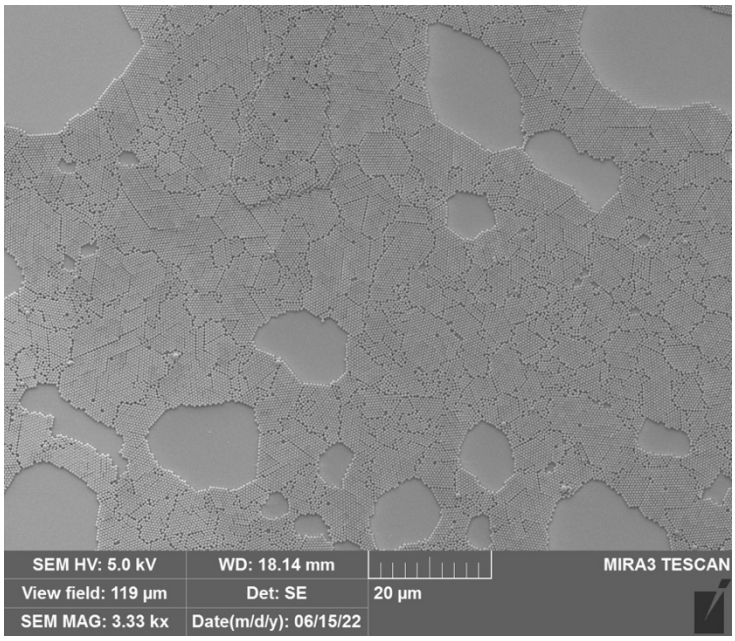

Figure A1. Monolayer of polystyrene spheres from a deposition with the surfactant solution (TX-100 : methanol, 1:400 v/v).

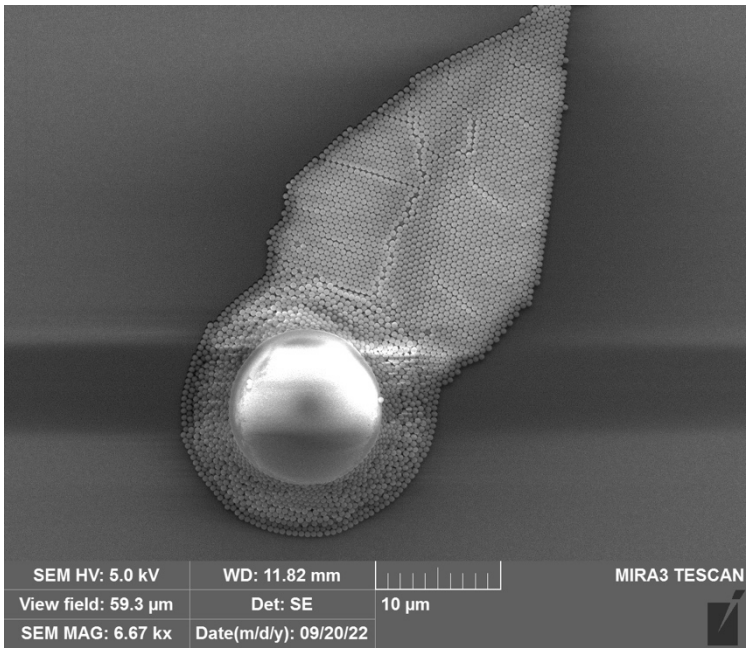

Figure A2. Structural defects in purchased polystyrene spheres gave larger spheres which had multilayers around them. This feature can negatively affect the LSPR signal and is termed the egg-feature in this paper

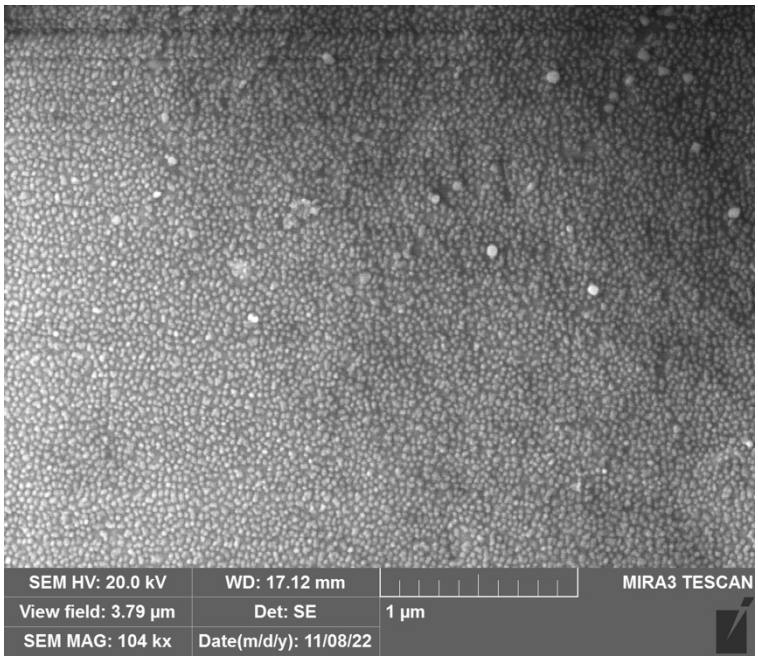

Figure A3. Scanning electron microscope of gold nanoparticles deposited on a glass cover slip

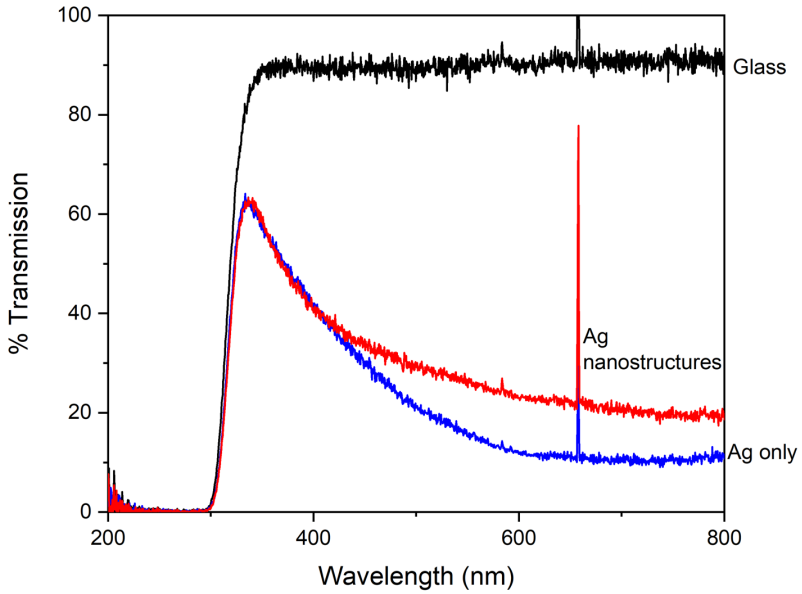

Figure A4. Overlay of the localised surface plasmon resonance spectra of HCP masks (red spectrum), silver deposited on glass (blue spectrum) and glass cover slip (black spectrum)

Table A1. Percent coverage values of area occupied by polystyrene spheres deposited on glass cover slips by centrifugal deposition. The data is for the two optimum ratios of sphere : surfactant solution and each value are for an individual sample from different batches.

	1:1 (%)	**2:1 (%)**	**3:1 (%)**
sample 1	16.5	29.1	25.7
sample 2	17.0	36.3	26.3
sample 3	18.4	48.8	25.1
sample 4	14.6	37.1	31.2
sample 5	21.9	38.9	35.4
sample 6	-	24.5	-
sample 7	-	35.4	-
sample 8	-	37.5	-
sample 9		27.2	
sample 10		28.9	
Average	**17.7**	**34.4**	**28.7**
Standard Deviation	**2.7**	**7.1**	**4.4**
RSD	**15.4**	**20.7**	**15.5**

Table A2. Percent reflectance values of various spots on samples of bare AgFONs. The λ_{max} of each sample's LSPR peak is indicated in the column titles.

Spot # on AgFON	**Sample 1 Peak 613 nm**	**Sample 2 Peak 615 nm**	**Sample 3 Peak 600 nm**
Spot 1	53.74	44.72	72.22
Spot 2	48.24	48.61	84.42
Spot 3	57.86	49.16	84.14
Spot 4	49.48	47.45	84.17
Spot 5	54.65	45.79	83.58
Spot 6	54.27	48.19	99.23
Spot 7	51.18	51.66	78.62
Spot 8	50.61	56.68	84.24
Spot 9	48.15	-	77.25
Spot 10	-	-	78.23
Spot 11	-	-	80.61
Average	**52.02**	**49.03**	**82.43**
Standard Deviation	**3.31**	**3.74**	**6.81**
RSD	**6.36**	**7.63**	**8.26**

Table A3. Percent reflectance values of the LSPR peaks of an AgFON samples with cardiac troponin I. Spectra of this sample is shown in Fig13a (black spectrum line).

AgFON + cTnI	Peak 513
spot1	13.58
spot2	14.90
spot3	17.96
spot4	19.28
spot5	12.59
spot6	12.48
spot7	12.14
spot8	10.37
spot9	16.21
Average	**14.39**
Standard Deviation	**2.94**
RSD	**20.41**

Table A4. Percent reflectance values of self-assembled monolayer (SAM) of thiol backfilling agents on an AgFON. The LSPR spectra of this sample is shown in Fig 18b (red spectrum line)

SAM + AgFON	Peak 600 - 615nm
spot1	88.39
spot2	87.25
spot3	79.95
spot4	78.29
spot5	84.91
spot6	81.28
spot7	81.96
spot8	89.75
Average	**83.97**
Standard Deviation	**4.21**
RSD	**5.02**

Table A5. Percent reflectance values of cardiac troponin I deposited on an AgFON with the self-assembled monolayer (SAM) of thiol backfilling agents. The LSPR spectra of this sample is shown in Fig13b (black spectrum line).

AGFON + SAM + cTnI	**Peak 530**	**Peak 498**
spot1	13.87	22.15
spot2	11.76	21.26
spot3	12.51	19.56
spot4	11.48	21.3
spot5	14.63	23.11
spot6	9.99	26.12
spot7	10.38	16.99
Average	**12.09**	**21.50**
Standard Deviation	**1.71**	**2.85**
RSD	**14.17**	**13.23**

Table A6. Reflectance values of aptamer mounted on AgFONs. LSPR peak is 522 nm (Fig14, red spectrum line) .

AgFON + Apt	**Peak 522 nm**	**Peak 341 nm**
1	57.63	36.74
2	73.22	53.3
3	85.83	51.35
4	79.71	39.04
5	75.12	50.97
6	78.48	50.25
7	60.52	42.45
8	82.52	43.6
Average	**74.13**	**45.96**
Standard Deviation	**10.12**	**6.29**
RSD	**13.65**	**13.69**

Table A7. Percent reflectance values of an AgFON modified with an aptamer and thiol backfilling agents. The LSPR peak is 522 nm, and the spectrum of this sample is shown on figure 14 (blue spectrum line).

AgFON + Apt + SAM	**522 nm**	**345 nm**
1	47	53.53
2	51	52
3	51.76	51.28
4	47.97	49.57
5	54.86	43.29
6	48.84	51.63
7	39.71	48.65
8	51.18	49.87
9	49.11	49.86
Average	**49.05**	**49.96**
Standard Deviation	**4.21**	**2.91**
RSD	**8.59**	**5.83**

Table *A8*. Percent reflectance values of cardiac troponin I on an AgFON modified with Tro4 aptamer and thiol backfilling agents. The LSPR peak is ~485 nm and the spectrum for this sample is shown in Fig 14 (green spectrum line).

AgFON + Apt + SAM + cTnI	**480-490 nm**	**343 nm**
1	36.01	39.9
2	42.68	38.14
3	43.72	36.98
4	44.63	43.77
5	31.7	36.25
6	42.15	46.34
7	46.59	40.5
8	26.14	25.24
9	23.64	27.13
Average	**37.47**	**37.14**
Standard Deviation	**8.50**	**6.99**
RSD	**22.68**	**18.83**

Electrochemical Aptasensor of Cardiac Troponin I for the Early Diagnosis of Acute Myocardial Infarction

Author: Hunho Jo, Hyunwoo Gu, Weejeong Jeon, et al
Publication: Analytical Chemistry
Publisher: American Chemical Society
Date: Oct 1, 2015

Copyright © 2015, American Chemical Society

PERMISSION/LICENSE IS GRANTED FOR YOUR ORDER AT NO CHARGE

This type of permission/license, instead of the standard Terms and Conditions, is sent to you because no fee is being charged for your order. Please note the following:

- Permission is granted for your request in both print and electronic formats, and translations.
- If figures and/or tables were requested, they may be adapted or used in part.
- Please print this page for your records and send a copy of it to your publisher/graduate school.
- Appropriate credit for the requested material should be given as follows: "Reprinted (adapted) with permission from {COMPLETE REFERENCE CITATION}. Copyright {YEAR} American Chemical Society." Insert appropriate information in place of the capitalized words.
- One-time permission is granted only for the use specified in your RightsLink request. No additional uses are granted (such as derivative works or other editions). For any uses, please submit a new request.

If credit is given to another source for the material you requested from RightsLink, permission must be obtained from that source.

BACK CLOSE WINDOW

Analytical applications of aptamers

Author: S. Tombelli,M. Minunni,M. Mascini
Publication: Biosensors and Bioelectronics
Publisher: Elsevier
Date: 15 June 2005

Copyright © 2004 Elsevier B.V. All rights reserved.

Order Completed

Thank you for your order.

This Agreement between Miss. Makatendeka Biton ("You") and Elsevier ("Elsevier") consists of your license details and the terms and conditions provided by Elsevier and Copyright Clearance Center.

Your confirmation email will contain your order number for future reference.

Printable Details

License Number	5521170271486
License date	Apr 03, 2023

Licensed Content

Licensed Content Publisher	Elsevier
Licensed Content Publication	Biosensors and Bioelectronics
Licensed Content Title	Analytical applications of aptamers
Licensed Content Author	S. Tombelli,M. Minunni,M. Mascini
Licensed Content Date	Jun 15, 2005
Licensed Content Volume	20
Licensed Content Issue	12
Licensed Content Pages	11

Order Details

Type of Use	reuse in a thesis/dissertation
Portion	figures/tables/illustrations
Number of figures/tables/illustrations	1
Format	electronic
Are you the author of this Elsevier article?	No
Will you be translating?	No

Cardiac troponin structure-function and the influence of hypertrophic cardiomyopathy associated mutations on modulation of contractility

Author: Yuanhua Cheng,Michael Regnier
Publication: Archives of Biochemistry and Biophysics
Publisher: Elsevier
Date: 1 July 2016

© 2016 Elsevier Inc. All rights reserved.

Order Completed

Thank you for your order.

This Agreement between Miss. Makatendeka Biton ("You") and Elsevier ("Elsevier") consists of your license details and the terms and conditions provided by Elsevier and Copyright Clearance Center.

Your confirmation email will contain your order number for future reference.

Printable Details

License Number	5521180148363
License date	Apr 03, 2023

Licensed Content

Licensed Content Publisher	Elsevier
Licensed Content Publication	Archives of Biochemistry and Biophysics
Licensed Content Title	Cardiac troponin structure-function and the influence of hypertrophic cardiomyopathy associated mutations on modulation of contractility
Licensed Content Author	Yuanhua Cheng,Michael Regnier
Licensed Content Date	Jul 1, 2016
Licensed Content Volume	601
Licensed Content Issue	n/a
Licensed Content Pages	11

Order Details

Type of Use	reuse in a thesis/dissertation
Portion	figures/tables/illustrations
Number of figures/tables/illustrations	1
Format	electronic
Are you the author of this Elsevier article?	No
Will you be translating?	No

About Your Work

Title	Developing A Localized Surface Plasmon Aptasensor for the Early Detection of Acute Myocardial Infarction
Institution name	Saint Mary's University
Expected presentation date	Apr 2023

Additional Data

Portions	Figure 3B

Requestor Location

Requestor Location	Miss. Makatendeka Biton 303 Washmill Lake Drive 408 Halifax, NS B3S 0J3 Canada Attn: SMU

Tax Details

Publisher Tax ID	GB 494 6272 12

Billing Address

Miss Makatendeka Biton
303 Washmill Lake Drive
408
Halifax, NS B3S 0J3
Canada

+1 (902) 580-8144
makatendeka.biton@smu.ca

Customer Location

Miss Makatendeka Biton
303 Washmill Lake Drive
408
Halifax, NS B3S 0J3
Canada

PO Number (optional)

N/A

Payment options

Invoice

PENDING ORDER CONFIRMATION

Confirmation Number: Pending
Order Date: 03-Apr-2023

Print Friendly Format

Includes Publisher Terms and Conditions

1. The analyst online

0.00 CAD

Article: Portable and field-deployed surface plasmon resonance and plasmonic sensors.

Order License ID	Pending	**Publisher**	Royal Society of Chemistry
ISSN	1364-5528	**Portion**	Image/photo/illustration
Type of Use	Republish in a thesis/dissertation		

View Details

Print License

Total Items: 1

Total Due: 0.00 CAD

Accepted: Marketplace Permissions General Terms and Conditions and any applicable Publisher Terms and Conditions

Continue Shopping